

TURKISH JOURNAL OF REMOTE SENSING
(Türkiye Uzaktan Algılama Dergisi)
e-ISSN 2687-4997
https://dergipark.org.tr/en/pub/tuzal

Multi-hazard risk mapping in mountainous microcatchments: Integrated avalanche-flood simulations with RAMMS and HEC-RAS

Alperen Meral[*1], **Engin Yıldız**[2]

[1] *Bingöl University, Faculty of Agriculture, Department of Landscape Architecture, Bingöl, Türkiye;* alperenmeral@gmail.com
[2] *General Directorate of Combating Desertification and Erosion, Department of Survey and Project, Ankara, Türkiye;* yildizengin90@gmail.com

Check for updates

Article History:
Received: 25 Dec. 2025
Revised: 20 Feb. 2026
Accepted: 3 May 2026
Published: 3 July 2026

Copyright: © 2026 by the authors.
This article is an open access article distributed under terms and conditions of the Creative Commons Attribution (CC BY-SA) license. https://creativecommons.org/licenses/by-sa/4.0/

Abstract: Climate change is intensifying the frequency and severity of extreme events such as avalanches and floods, particularly in mountainous regions where these hazards may develop concurrently and interactively. Despite growing recognition of the need for integrated risk management, most previous studies have assessed avalanche and flood hazards in isolation. This study presents a microcatchment-scale, physically based multi-hazard modeling framework that combines the RAMMS and HEC-RAS models to assess compound avalanche–flood risks in the Lediz Microcatchment (Bingöl Province, Türkiye), a representative high-risk mountainous basin. Avalanche simulations were performed using RAMMS with validated release areas and flow dynamics, while flood hazards were modeled using 2D HEC-RAS simulations calibrated against historical events and stakeholder observations. Results revealed substantial spatial overlap between high to very high avalanche risk zones and extreme flood hazard areas, particularly affecting settlements such as Dereköy, Şehittepe, Şin, Balgöze, Işıklı, and Palacık. Zones exceeding 15 m/s in avalanche velocity, 100 kPa in dynamic pressure, and flood hazard rating (HR), defined as a function of flow depth and velocity (HR = d × (v + 0.5)), exceeding 2.5, indicate severe structural and socio-economic vulnerability. The findings underscore the critical need to integrate multi-hazard analysis into spatial planning and disaster risk reduction policies, with a particular focus on vulnerable rural landscapes. This study provides a scalable and adaptable modeling framework for identifying compound hazard hotspots, offering novel insights for risk-informed land-use planning and resilience-based disaster management in climate-sensitive mountainous environments.

Keywords: Mountain microcatchment; RAMMS; HEC-RAS; flood modeling; avalanche simulation

Citation: Meral A., & Yıldız E. (2026). Multi-hazard risk mapping in mountainous microcatchments: integrated avalanche-flood simulations with RAMMS and HEC-RAS. *Turk. J. of Remote Sens.* 8, 1848947. https://doi.org/10.51489/tuzal.1848947

1. Introduction

Human interactions with extreme natural events and hazards are increasing globally (Fuchs et al., 2015; Yousefi et al., 2020). Across the world, landscapes are shaped as reflections of diverse natural processes. The likelihood of extreme events is particularly high in natural areas, where such phenomena often represent intrinsic components of natural systems (Bell & Glade, 2004). However, by employing predictive methods grounded in novel approaches and more comprehensive information about contributing factors, it is possible to significantly reduce human exposure to these hazards (Lee et al., 2024).

Watershed-scale modeling provides a critical framework for understanding and mitigating the complex interactions between avalanche and flood risks, particularly in multi-hazard-sensitive landscapes (Pearson, 2016). A standardized approach enables the holistic and robust assessment of multi-hazard risks, allowing outcomes to be directly compared with predefined risk tolerance thresholds. This facilitates more effective communication of risk to stakeholders and supports the prioritization of risk management strategies addressing multiple geohazards (Argue et al., 2023). Multi-hazard exposure mapping is a key tool for enhancing resilience through nature-based approaches. In mountainous regions

especially, it plays a vital role in managing hazard dynamics and ensuring the long-term sustainability of local ecosystems and communities (Barbolini et al., 2011; Rahmati et al., 2019; Van Westen & Greiving, 2017). Resilient socio-ecological systems possess the capacity to adapt and apply relevant knowledge to disaster risk reduction, while self-organizing to develop nature-based and risk-sensitive infrastructures (Rahmati et al., 2019; Zhou et al., 2010). Encouragingly, the significance of multi-hazard exposure analysis is increasingly being recognized, as hazard-focused perspectives and policies gradually evolve toward risk-based management frameworks across various global regions (Jaafari et al., 2024; Youssef et al., 2022). While research on individual hazards has reached a high level of maturity, single-hazard-based assessments often yield incomplete or inadequate outcomes in contexts where multiple hazards occur simultaneously. This is primarily because multi-hazard risk analyses are not merely the sum of individual hazard assessments; instead, they represent complex processes involving interacting and cascading effects (Kappes et al., 2012; Wang et al., 2020). Therefore, ensuring the comparability and interoperability of individual hazard analyses is essential for conducting accurate and meaningful multi-hazard risk assessments (Marzocchi et al., 2009; Tarvainen et al., 2006).

Traditionally, avalanche and flood risks have been examined largely in isolation. However, recent studies have demonstrated that these two hazards can interact both spatially and temporally, particularly in mountainous regions (Gariano & Guzzetti, 2016; Martha et al., 2021; Rusk et al., 2022). For instance, heavy snowfall can lead to the accumulation of large snow masses, which, when followed by sudden temperature increases or rainfall, may trigger avalanches and simultaneously enhance flood risk through snowmelt and surface runoff (Terzi et al., 2019; Yousefi et al., 2020). Such concurrent hazard events increase the complexity of emergency response planning and underscore the need for integrated approaches in disaster risk management policies (Gill & Malamud, 2014).

Mountainous regions are commonly affected by a variety of natural hazards, including snow avalanches (Fuchs et al., 2015; Pearson, 2016), landslides (Fuchs et al., 2015; Suresh D. et al., 2019), floods (Barredo, 2007; Rahmati et al., 2016), mudflows (Tsereteli et al., 2019), ice avalanches (Corona & Stoffel, 2017), soil erosion (Gayen & Pourghasemi, 2019; Pardini et al., 2003; Prosdocimi et al., 2016), rockfalls (Michoud et al., 2012), and wildfires (Abatzoglou & Kolden, 2013; Eskandari & Chuvieco, 2015; Gigović et al., 2019; Le Page et al., 2008; Pourghasemi, 2016; Pourtaghi et al., 2016). Despite the presence of multiple hazardous processes affecting the same landscape, most studies tend to focus on a single hazard (Amiri & Eslamian, 2010; Gigović et al., 2019; Haigh et al., 1995; Hand et al., 2004; Pourghasemi et al., 2017; Rijsdijk et al., 2007; Spitz et al., 2001; Yousefi et al., 2020).

Climate change-induced increases in extreme weather events are significantly intensifying disaster risks, particularly in mountainous and coastal regions. This trend highlights the vulnerability of both natural systems and human settlements, underscoring the necessity of multi-hazard risk assessments. For instance, during the winter of 2014, the United Kingdom (especially Scotland) experienced a series of severe storms that resulted in widespread damage due to high winds, extensive flooding, and avalanches (Met Office, 2014; Tilloy et al., 2019). Such events demonstrate the devastating potential of simultaneous multi-hazard impacts and emphasize the urgent need for integrated risk management approaches.

Although this study does not directly incorporate climate change scenario modeling, recent literature provides strong evidence that climate variability amplifies the frequency and intensity of snow avalanches and floods in mountain regions. Increases in extreme precipitation events, rapid warming episodes, and anomalous snowfall have been directly linked to the rising occurrence of such hazards (Ballesteros-Cánovas et al., 2018; Gariano & Guzzetti, 2016; Terzi et al., 2019; Zscheischler et al., 2018). Compound events, where avalanches and floods interact spatially or temporally, are increasingly recognized as climate-driven processes (Ebi, 2025). Regional climate projections for Eastern Anatolia further indicate greater variability in snow accumulation and melt dynamics, suggesting that

climate change will continue to shape multi-hazard regimes in this area (Demircan et al., 2017; Mesta et al., 2022). Therefore, while climate change is not explicitly analyzed here, it provides an essential contextual driver for understanding the hazard interactions assessed in the Lediz Microcatchment.

In this context, strategies that combine multi-hazard analyses with nature-based solutions play a pivotal role in building more resilient socio-ecological systems against disasters. Despite the increasing recognition of multi-hazard interactions in mountainous environments, a significant research gap remains in the integrated assessment of avalanche and flood processes at the microcatchment scale. Existing studies predominantly adopt single-hazard approaches, which fail to capture the nonlinear interactions, cascading effects, and spatial overlaps that characterize compound hazard systems. Moreover, physically based modeling frameworks are rarely applied in a coupled manner to simultaneously evaluate gravitational and hydrodynamic processes within the same spatial context.

This study addresses this critical gap by developing a microcatchment-scale, physically based multi-hazard modeling framework that integrates RAMMS avalanche simulations with 2D HEC-RAS flood modeling. The novelty of this research lies in (i) the explicit spatial coupling of avalanche and flood hazard outputs, (ii) the identification of compound hazard hotspots based on physically derived thresholds, and (iii) the integration of these results into a risk-informed spatial planning perspective. By moving beyond conventional single-hazard assessments, this study provides a transferable and scalable methodological framework for understanding compound hazard dynamics in climate-sensitive mountainous regions.

2. Materials and Methods

2.1. Research area

The Lediz Microcatchment, located within the boundaries of Genç District in Bingöl Province, was selected as the study area. From both hydrological and topographical perspectives, the Lediz Microcatchment is considered one of Turkey's high-risk mountainous catchments. These characteristics make it a suitable case for modeling multiple natural hazard risks. The basin features steep slopes, narrow valleys, areas with high snow accumulation potential, and a seasonally variable flow regime. Such conditions create a critical natural system where the simultaneous occurrence of flood and avalanche events can be triggered, particularly during periods of intense precipitation and snowmelt (Figure 1).

Post-1980 climate data from the Lediz Microcatchment reveal a frequent overlap of snowfall, sudden warming events, and intense precipitation, creating a hazard-prone environment where avalanches and floods may develop interactively. Moreover, settlements, agricultural lands, and forested areas surrounding Lediz are highly exposed to these natural hazards. In this context, the region offers a suitable natural laboratory for flood modeling using HEC-RAS and avalanche scenario simulations with RAMMS.

The Lediz Microcatchment, located within the Genç district of Bingöl Province, includes the villages of Sürekli, Ardıçdibi, Şehittepe, Dereköy, Balgöze, and Yiğitbaşı, as well as the Parçançkomu and Koyuncu hamlets of Keklikdere Village, and the Mutluca hamlet of Meşedalı Village. The elevation of the basin ranges from 1,020 to 2,370 meters, with an average elevation of approximately 1,500 meters. The area receives an average annual precipitation of 831 mm, experiences about 117 days of snowfall, and remains snow-covered for approximately 76 days annually (Baydaş et al., 2018; OGM, 2013).

In addition to its geomorphological characteristics, the Lediz Microcatchment has experienced several flood events driven by the combined effects of intense precipitation and rapid snowmelt, with the 2020 Şehittepe flood representing a well-documented case of localized inundation and infrastructure damage. The basin is characterized by a snowmelt–rainfall dominated hydrological regime, with an average annual precipitation of approximately 831 mm and seasonal snow cover persisting for up to 76 days (Baydaş et al.,

2018; OGM, 2013). Rapid temperature increases during late winter and early spring frequently accelerate snowmelt processes, often coinciding with high-intensity rainfall events, thereby amplifying surface runoff and peak discharge generation. Regional climate projections further indicate increasing variability in extreme precipitation and short-duration rainfall events in Eastern Anatolia (Demircan et al., 2017; Mesta et al., 2022). These hydro-meteorological characteristics indicate that the basin operates under a highly dynamic regime where rapid shifts between snow accumulation and melt processes can trigger nonlinear hazard responses, thereby increasing the likelihood of compound avalanche–flood interactions.

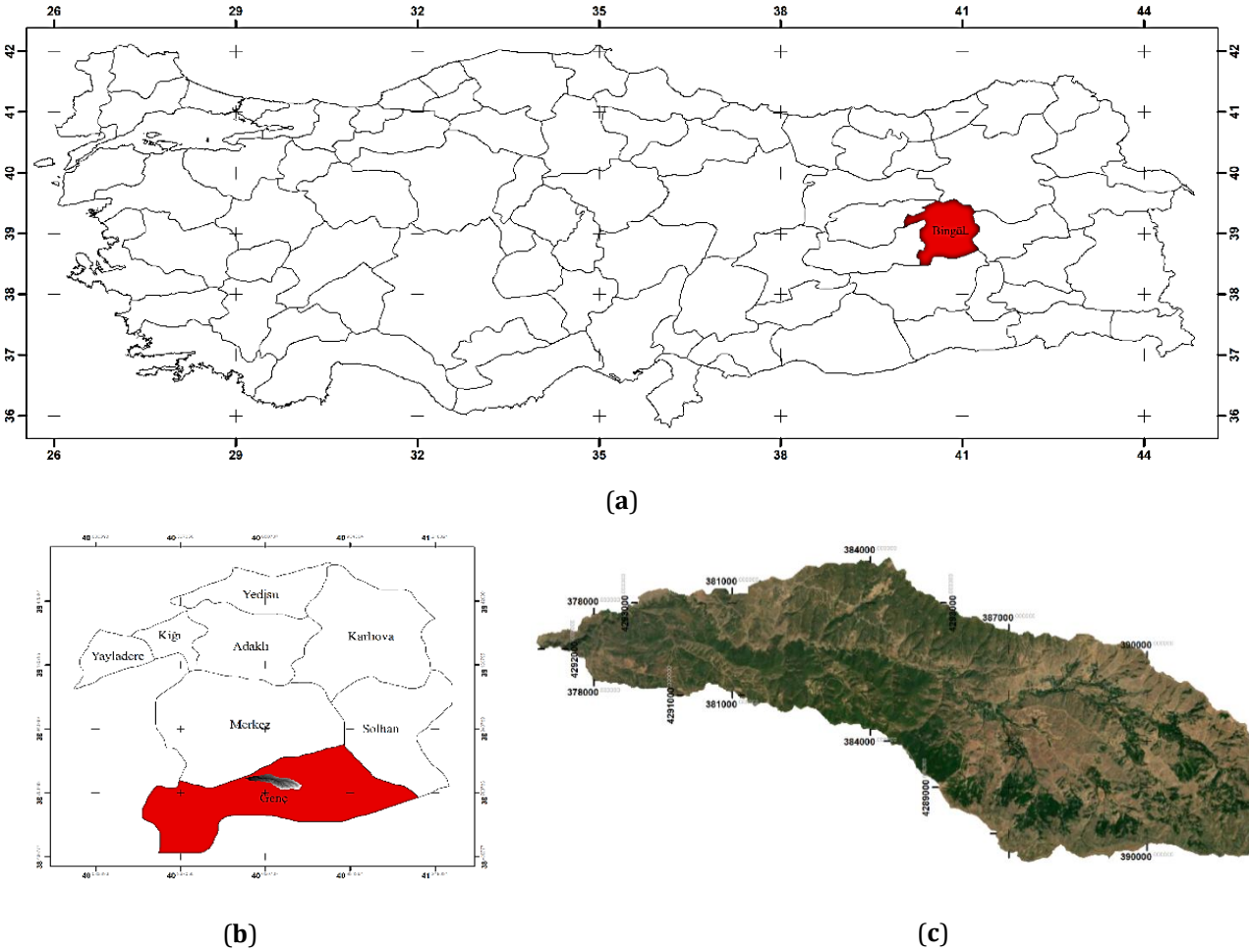


Figure 1. The location of Bingöl Province within the national context of Türkiye (a), the regional position of the Genç District within Bingöl Province (b), and the satellite-based boundaries of the designated study area (c)

2.2. Physiographic, geological, and hydro-meteorological characteristics of the Lediz microcatchment

Figure 2 presents a set of thematic maps illustrating the key physiographic and geological features of the Lediz Microcatchment. The slope and curvature maps highlight the steep terrain and complex surface morphology that strongly influences runoff generation, avalanche initiation, and flood dynamics. The aspect and elevation maps emphasize the altitudinal variability and orientation of the basin, which are critical for understanding snow accumulation, melt processes, and microclimatic conditions. The geological map delineates the dominance of Precambrian gneiss and schist units, reflecting the low-permeability metamorphic basement that governs surface hydrology and slope stability. In addition, land capability classification indicates that the majority of the basin falls within Class VII, representing areas with severe limitations that are unsuitable for cultivation and highly

prone to degradation. Together, these maps provide a spatially explicit foundation for assessing multi-hazard interactions within the basin.

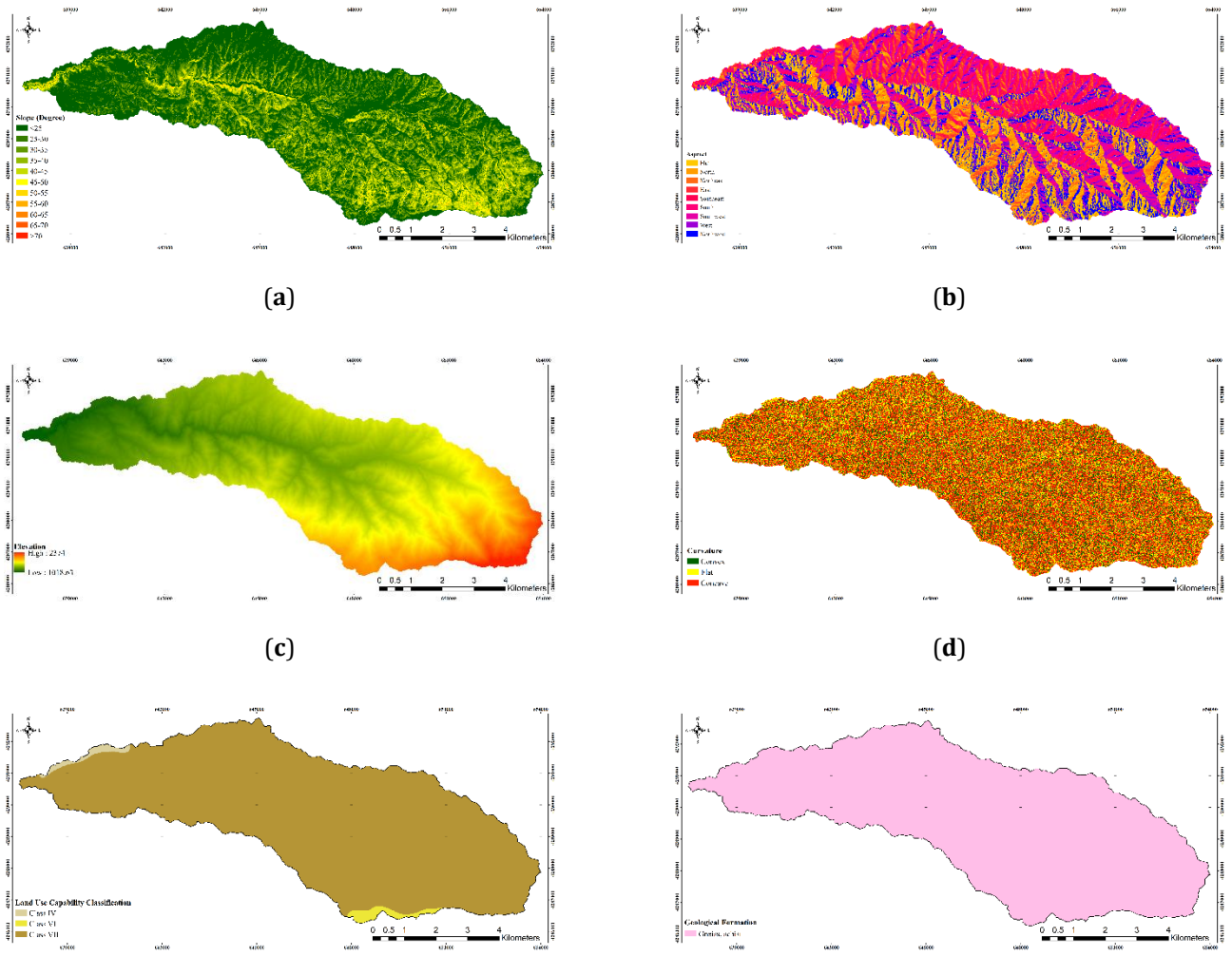


Figure 2. Thematic maps illustrating the physiographic and geological characteristics of the Lediz Microcatchment: (a) slope, (b) aspect, (c) elevation, (d) curvature, (e) land capability classification and (f) geological map

To complement the spatial information provided by the thematic maps, the key morphometric, geological, and hydro-meteorological parameters of the Lediz Microcatchment were quantified and are summarized in Table 1. These parameters include basin area, drainage density, stream frequency, basin shape index, relief ratio, aspect distribution, and flow regime characteristics, alongside lithological and climatic descriptors. The results highlight the dominance of steep slopes, low-permeability Precambrian gneiss–schist formations, and a snowmelt–rainfall driven flashy hydrological regime. Land capability classification further indicates that much of the basin falls within Class VII, with severe land-use limitations. Collectively, these characteristics underline the basin's pronounced susceptibility to rapid runoff generation and multi-hazard interactions, thereby providing a robust foundation for subsequent avalanche–flood modeling.

The Digital Elevation Model (DEM) used in this study was generated from 1:25,000 scale topographic maps by digitizing contour lines at 10 m intervals and constructing a Triangulated Irregular Network (TIN) surface. The TIN was subsequently converted into a raster DEM with a 10 m spatial resolution to ensure compatibility with the 2D HEC-RAS computational grid. Prior to hydraulic simulation, the DEM underwent hydrological

conditioning, including sink filling and surface smoothing procedures in ArcGIS Pro, to eliminate artificial depressions and ensure realistic flow routing dynamics. This high-resolution terrain representation was essential for accurately capturing channel confinement and slope-controlled flow behavior in the narrow valleys of the Lediz Microcatchment.

Table 1. Key morphometric, geological, and hydro-meteorological parameters of the Lediz microcatchment

Category	Parameter	Value / Description	Source / Notes
Morphometric	Basin Area (km^2)	51.00	DEM-derived
	Basin Length (km)	14.85	DEM-derived
	Basin Width (km)	3.54	DEM-derived
	Drainage Density (km/km^2)	2.13	$Dd = \frac{L}{A}$
	Stream Frequency (F_s)	0.78	$F_s = \frac{N}{A}$
	Basin Shape Index (F_f)	0.23	$F_f = \frac{A}{L_b^2}$
	Relief Ratio (Rh)	0.091 (H = 1355.49 m; L = 14.85 km)	$Rh = \frac{AH}{L_b}$
	Aspect Distribution	Dominant SW–NW and W-facing slopes	DEM-derived
	Elevation (Mean)	1159,64 m (Min = 1018,62 m; Max = 2374,11 m)	DEM-derived
	% Slope (Mean)	52,63 % ((Min = 0,00 %; Max = 294,75 %)	DEM-derived
Geological	Dominant Lithology	Metamorphic units (gneiss, schist)	(MTA, 2025)
	Rock Type	Precambrian gneiss and schist	(MTA, 2025)
	Structural Features	Fault zones present	(MTA, 2025)
Meteorological	Mean Annual Precipitation	831 mm	(Baydaş et al., 2018)
	Annual Snowfall Duration	117 days	(Baydaş et al., 2018)
	Snow Cover Duration	~76 days	(OGM, 2013)
	Mean Annual Temperature	~7–9 °C (regional)	(MGM, 2025)
Hydrological	Main River	Lediz Stream (tributary of Murat River)	(OGM, 2013)
	Flow Regime	Snowmelt–rainfall dominated flashy regime, with rapid runoff due to steep slopes, moderate–high drainage density, and low-permeability Precambrian basement rocks	Integrated analysis
Land Capability	Classification	Class VII – severe limitations, unsuitable for cultivation	Regional land capability data

The morphometric parameters presented in Table 1 indicate that the Lediz Microcatchment is a relatively small but topographically rugged basin with steep slopes and a pronounced relief ratio (0.091). The low form factor (0.23) suggests an elongated basin shape, which generally results in longer concentration times but, when combined with the moderate–high drainage density (2.13 km/km^2) and stream frequency (0.78 km^{-2}), still favors rapid runoff generation. The predominance of southwest–west–northwest facing slopes highlights the role of aspect in snow accumulation and meltwater dynamics. The geological setting, dominated by low-permeability Precambrian gneiss and schist, restricts infiltration and further accelerates overland flow. Together with the basin's Class VII land capability classification, these characteristics emphasize the limited land-use potential and high susceptibility of the catchment to accelerated runoff, erosion, and compound avalanche–flood hazards.

2.3. Microcatchment-scale multi-hazard modeling approach

2.3.1. Avalanche simulation using the RAMMS model

In this study, avalanche hazard modeling was conducted using the RAMMS::AVALANCHE module, developed by the WSL Institute for Snow and Avalanche Research (SLF) in Switzerland. RAMMS (Rapid Mass Movement Simulation) is a state-of-the-art, physically based, two-dimensional numerical model tailored for simulating rapid mass movement processes. The model solves depth-averaged mass and momentum conservation equations derived from shallow water theory, effectively capturing avalanche dynamics across complex mountainous topographies (Christen et al., 2010; Dillon & Hammonds, 2021; Yıldız & Bulut, 2024).

The simulation framework incorporates terrain morphology via a high-resolution digital elevation model (DEM) and accounts for key surface interaction parameters such as basal friction and terrain roughness. RAMMS applies a Voellmy-type friction law that combines a dry Coulomb friction coefficient (μ) with a turbulent friction term (ξ), thereby enabling robust simulation of both dry-snow avalanches and wet-flow events characterized by high-density, energy-dissipative behavior (Bartelt et al., 2017; RAMMS, 2024).

Model input parameters (including snow cover thickness, snowpack density, and slab volume) were parameterized for each potential release area based on in-situ terrain surveys and meteorological records. Simulations were executed under both historical-event scenarios and worst-case conditions to delineate potential avalanche runout zones and assess dynamic outputs such as maximum flow velocity, flow depth, and pressure distribution (Koçyiğit et al., 2016).

Following the simulation, a hazard classification scheme was developed and used to construct a four-tier avalanche risk map tailored to the geomorphological and settlement characteristics of the microcatchment area (Table 2). This risk zoning provides a spatially explicit framework for integrated hazard mitigation and land-use planning in avalanche-prone terrains.

Table 2. Avalanche Risk Classification Scheme (Christen et al., 2010; Gruber & Bartelt, 2007; RAMMS, 2024)

Risk Level	Max. Velocity (m/s)	Pressure (kPa)	Max. Flow Height (m)	Impact Description
Low	<5	<5	<0.50	Minor snow movement with low risk to pedestrians. Limited impact on trees and roads.
Moderate	5–15	5–30	0.50–1.50	Risk to small structures and vehicles. Potential damage to agricultural land.
Significant	15–25	30–100	1.50–3.00	Damage to medium-sized buildings, power lines, and critical infrastructure. High risk of fatalities.
Extreme	>25	>100	>3.00	Complete destruction of large structures. Lethal threat to residential areas; mandatory evacuation required.

The primary outputs derived from the RAMMS simulations include:

- Flow depth (m)
- Velocity (m/s)
- Dynamic pressure (kPa), calculated as $0.5 \cdot \rho \cdot v^2$

These outputs were integrated with high-resolution land use data and exposure metrics to delineate avalanche hazard zones (Z1–Z4) across the study area (Figure 3). The resulting zonation serves as a quantitative spatial framework for multi-parametric hazard assessment, enabling detailed analysis of spatial variability in avalanche dynamics and facilitating scenario-based risk modeling for complex terrain environments. The hazard zoning framework (Z1–Z4) was directly derived from model-based physical thresholds including maximum velocity, impact pressure, and flow height. To ensure visual-methodological

consistency, the legend classifications in the final avalanche hazard maps strictly correspond to the defined matrix categories (Low, Moderate, Significant, Extreme). This alignment eliminates interpretative discrepancies between theoretical classification and spatial representation. In order to ensure terminological consistency between the classification matrix and the spatial outputs, the legend categories used in the avalanche hazard maps (Low, Moderate, Significant, Extreme) directly correspond to Z1–Z4 classes defined in Table 2. Although minor wording differences may appear between the matrix representation and map legends, the thresholds remain physically identical, thereby preserving methodological coherence between conceptual zoning and spatial simulation results.

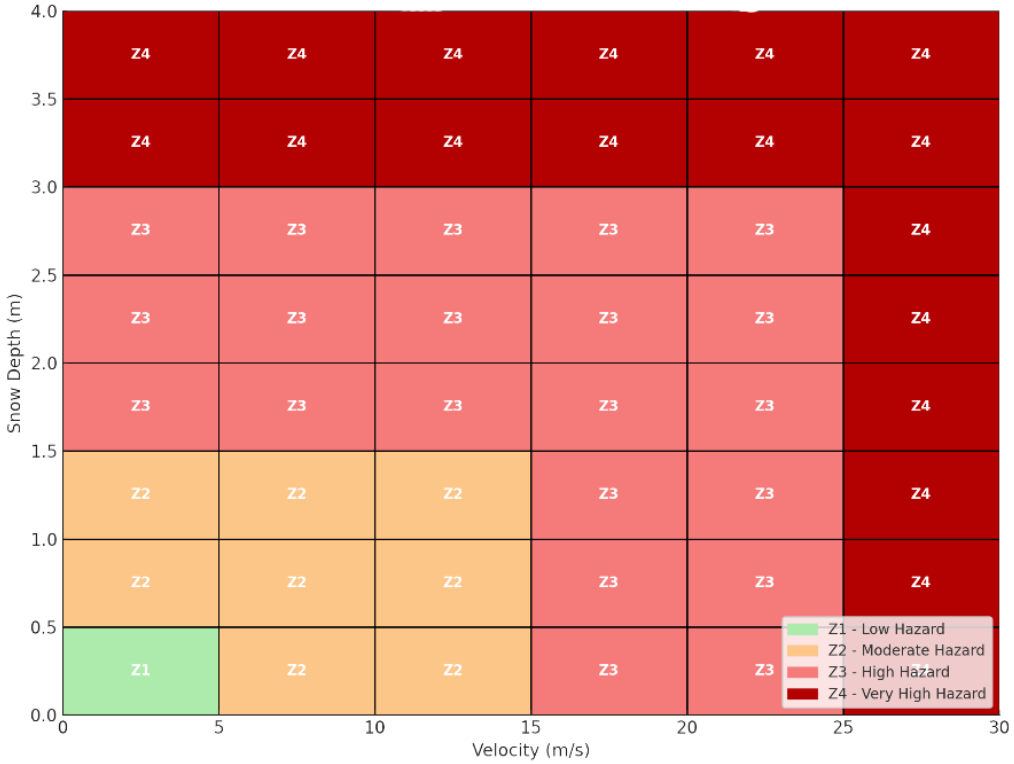


Figure 3. Avalanche hazard classification matrix (Z1 Low Hazard, Z2 Moderate Hazard, Z3 Significant Hazard, Z4 Extreme Hazard)

In the current graph, only snow depth (Y-axis) and avalanche velocity (X-axis) are visualized. Dynamic pressure was considered during the classification process but was not explicitly presented as a third axis or color scale within the visual output.

The delineation of avalanche release areas exerts a critical influence on the final stage of avalanche risk analysis performed with the RAMMS model. According to the literature, key geomorphometric parameters controlling release zone location include mean slope angle, terrain curvature index, and ridge proximity index. Increased slope gradients have been shown to significantly elevate the frequency of small avalanche occurrences (Bulut et al., 2024; Demir, 2018; Maggioni & Gruber, 2003; Meral & Yüksel, 2024; Yıldız & Bulut, 2024).

Maggioni et al. (2002) developed an algorithm for identifying potential avalanche release areas using a dataset of 4,500 recorded avalanche events from the Davos region of Switzerland. The same algorithm is applied in this study to delineate release zones. The algorithm integrates the following terrain metrics:

- Slope angle between 30° and 60°;
- High ridge proximity index, indicating primary flow partitioning and initiation zones;
- Concave terrain curvature index (negative plan curvature), favoring slab formation;
- Terrain aspect orientation relative to prevailing wind and insolation patterns.

Following the identification of release areas, a 100-year return period avalanche simulation was conducted using the RAMMS::AVALANCHE module, with subsequent mapping of potential avalanche impact extents. The RAMMS::AVALANCHE module is specifically engineered to simulate gravity-driven rapid mass movements such as avalanches. It calculates key flow parameters along three-dimensional flow paths, from initiation zones through complex terrain, by solving depth-averaged dynamic equations (Bartelt et al., 2017; Bütün & Koçyiğit, 2019). The methodological workflow adopted for the avalanche simulations is detailed in Figure 4. Such an approach ensures robust representation of terrain-controlled release dynamics, thereby enhancing the reliability and spatial accuracy of subsequent flow simulations. While RAMMS provides highly reliable flow dynamics modeling, the accuracy of release zone delineation remains a key determinant of overall model performance (Bartelt et al., 2017).

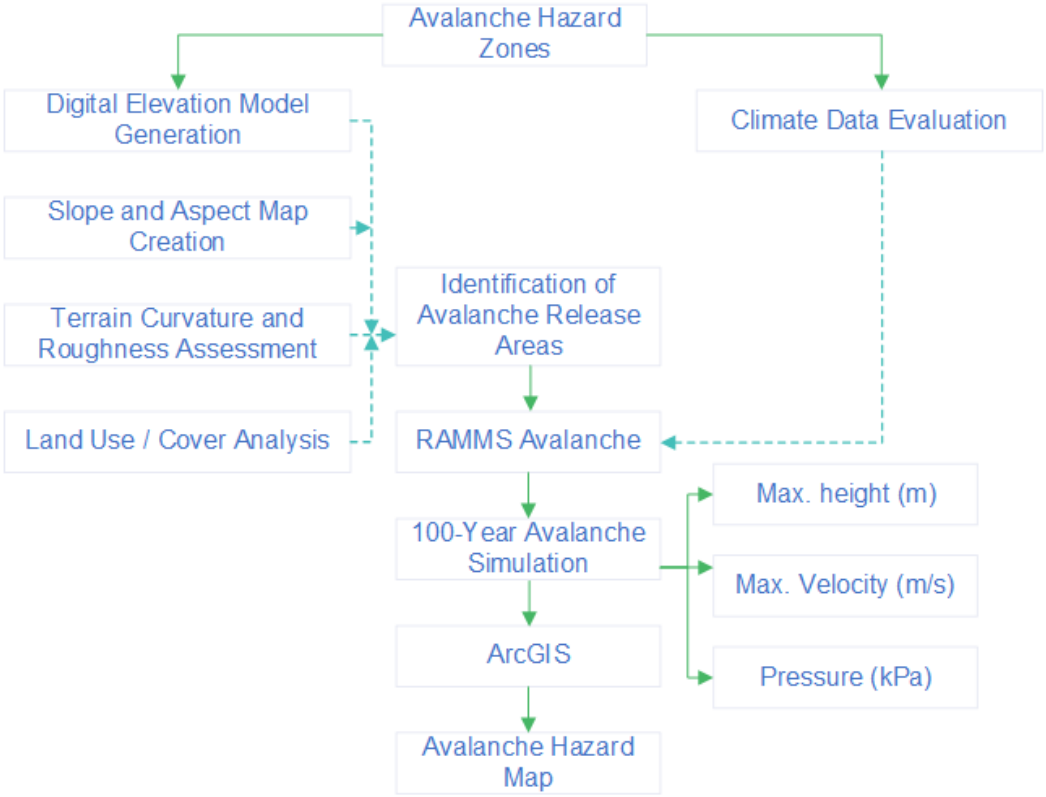


Figure 4. Methodological workflow for delineating release areas and simulating avalanche flow dynamics using the RAMMS::AVALANCHE module (Bütün & Koçyiğit, 2019; Meral & Yüksel, 2024; Yıldız & Bulut, 2024)

2.3.2. Flood simulation using the HEC-RAS model

HEC-RAS (Hydrologic Engineering Center's River Analysis System) is a widely used hydraulic modeling software developed by the U.S. Army Corps of Engineers. Designed to simulate water flow in natural river systems and artificial channels, the software enables the development of both one-dimensional and two-dimensional models under steady and unsteady flow conditions (Duvvuri & Narasimhan, 2013; Lamichhane & Sharma, 2018; USACE, 2010). HEC-RAS is extensively applied in floodplain mapping and flood risk analysis by calculating hydraulic parameters such as water surface profiles, flow depth, and velocity. Additionally, the software is capable of modeling sediment transport and the dispersion of chemical pollutants, thereby facilitating comprehensive riverine process and water quality analyses (AL-Hussein et al., 2022; Duvvuri & Narasimhan, 2013; Maidment, 2017). For unsteady flow simulations, HEC-RAS employs flood routing techniques based on the St.

Venant equations of mass and momentum conservation (Ackerman et al., 2008; Bharath et al., 2021; Leandro & Martins, 2016; Pathan & Agnihotri, 2021).

In this study, flood hazards were simulated using the 2D unsteady flow module of HEC-RAS. The 2D solver is based on the depth-averaged Saint-Venant (shallow water) equations, ensuring conservation of mass and momentum in both horizontal directions (Chow, 1959; Toro, 2001; Brunner, 1995; USACE, 2023). In compact form, the governing equations can be expressed as Equation 1-3.

$$\frac{\partial h}{\partial t} + \frac{\partial (hu)}{\partial x} + \frac{\partial (hv)}{\partial y} = q \tag{1}$$

$$\frac{\partial (hu)}{\partial t} + \frac{\partial (hu^2 + 1/2gh^2)}{\partial x} + \frac{\partial (huv)}{\partial y} = gh(S_{0x} - S_{fx}) \tag{2}$$

$$\frac{\partial (hv)}{\partial t} + \frac{\partial (huv)}{\partial x} + \frac{\partial (hv^2 + 1/2gh^2)}{\partial y} = gh(S_{0y} - S_{fy}) \tag{3}$$

where h is water depth, u and v are depth-averaged velocity components in the x and y directions, g is gravitational acceleration, q represents lateral inflow/outflow per unit area, S_{0x} and S_{0y} represent bed slope components in the x and y directions, while Sf denotes the friction slope.

For completeness, the one-dimensional form of the unsteady Saint-Venant equations (often presented as the theoretical basis for open-channel unsteady flow) is provided below. These 1D equations represent an along-channel reduction of the governing shallow-water framework and are commonly used to describe unsteady routing in prismatic channel assumptions Equation 4-5.

$$\frac{\partial A}{\partial t} + \frac{\partial Q}{\partial x} = 0 \tag{4}$$

$$\frac{\partial Q}{\partial t} + \frac{\partial}{\partial x}\left(\frac{Q^2}{A}\right) + gA\left(\frac{\partial z}{\partial x} + S_f - S_e\right) = 0 \tag{5}$$

where Q is discharge, A is cross-sectional flow area, t is time, z is water surface elevation relative to a datum, Sf is friction slope, and Se represents energy losses associated with expansion or contraction.

Accordingly, while the present study implements the 2D unsteady solver in HEC-RAS to represent lateral spreading and complex valley hydraulics, the 1D equations are retained here solely to clarify the classical theoretical formulation of unsteady open-channel flow.

The two-dimensional hydraulic simulations were conducted using the unsteady flow module of HEC-RAS, which applies a finite-volume numerical scheme to solve the depth-averaged Saint-Venant (shallow water) equations over a computational mesh (Brunner, 1995; USACE, 2023). The solver employs a semi-implicit formulation that enhances numerical stability under rapidly varying flow conditions and steep bed gradients, which are characteristic of mountainous microcatchments (Leandro & Martins, 2016; Toro, 2001).

The computational domain encompassed the main channel of the Lediz Stream together with adjacent floodplain areas to adequately represent potential lateral flow expansion during extreme discharge events. A structured two-dimensional mesh with a uniform spatial resolution of 10 m was generated, consistent with the resolution of the hydrologically conditioned DEM. The selected grid size represents a compromise between computational efficiency and topographic representation accuracy, as mesh resolution directly influences flood extent prediction and velocity distribution in high-relief terrain (Horritt & Bates, 2002; Teng et al., 2017).

The upstream boundary condition was defined using a design hydrograph corresponding to the 100-year return period flood event (Q100). The hydrograph was implemented as a discharge time-series at the upstream inflow cells of the 2D domain and

reflects compound snowmelt–rainfall processes typical of Eastern Anatolian high-relief basins. At the downstream boundary, a normal depth condition was imposed using the energy slope derived from the longitudinal channel gradient extracted from the DEM. This approach ensures physically consistent outlet control under unsteady flow conditions and is widely adopted in open-channel hydraulic modeling where stage measurements are unavailable (Chow, 1959; Brunner, 1995).

Simulations were performed under fully unsteady flow conditions. The computational time step was selected according to the Courant–Friedrichs–Lewy (CFL) stability criterion, expressed as Equation 6.

$$C = \frac{v\Delta t}{\Delta x'} \tag{6}$$

where v denotes flow velocity, Δt the computational time step, and Δx the grid resolution. Courant numbers were maintained below unity to ensure numerical stability and to minimize spurious oscillations in steep-gradient flow regions (Toro, 2001; USACE, 2023). Sensitivity analyses were conducted by varying Manning's roughness coefficients within the range 0.03–0.07 and adjusting peak inflow magnitudes to evaluate model responsiveness to hydraulic parameter uncertainty. The simulations demonstrated stable convergence behavior and consistent inundation patterns across parameter ranges, indicating numerical robustness of the hydraulic configuration.

Manning's roughness coefficients (n) were assigned based on CORINE Land Cover classes and supported by field observations. As n is an empirical parameter influenced by surface material, vegetation, and channel irregularity, its selection was guided by established hydraulic references (Chow, 1959; Arcement & Schneider, 1989). The selected range (0.035–0.10) is consistent with gravel-bed channels and semi-urban floodplains. In addition, the approach is aligned with recent studies employing the Cowan method combined with remote sensing for spatially distributed roughness estimation (Demir & Keskin, 2019), ensuring both physical realism and spatial consistency in the hydraulic simulations. A sensitivity analysis indicated that variations in Manning's n within plausible ranges resulted in changes of approximately 10–12% in simulated water depth, confirming the robustness of the model outputs.

To evaluate model performance, validation was performed using the documented 2020 Şehittepe flood event. Observed flood extents were digitized from municipal damage records, post-event field documentation, and photographic evidence. A GIS-based spatial overlay analysis was performed to quantify spatial agreement between modeled and observed flood extents. The overlap metric was calculated as the ratio of intersecting inundation area to the union of observed and modeled flood extents. The spatial overlap ratio reached approximately 76%, indicating satisfactory performance for microcatchment-scale 2D hydraulic modeling in steep topographic settings. Spatial agreement between the modeled and observed inundation extents was quantified using an overlap index, which measures the ratio of intersecting flood areas to the union of both spatial datasets (Equation 7).

$$Overlap = \frac{A_{observed} \cap A_{simulated}}{A_{observed} \cup A_{simulated}} \tag{7}$$

The spatial overlap ratio reached approximately 76%, indicating satisfactory predictive capability for microcatchment-scale 2D hydraulic modeling in steep mountainous environments. Comparable levels of agreement have been reported in similar high-relief flood modeling studies employing depth-averaged shallow-water solvers (Costabile et al., 2009; Teng et al., 2017).

In addition to spatial comparison, qualitative validation was supported through assessment of simulated maximum water depths against observed flood marks and reported impact zones within settlement areas. The modeled depth distribution and flow pathways

were consistent with documented damage patterns, reinforcing the physical plausibility of the hydraulic outputs.

No artificial hydraulic structures (e.g., bridges or culverts) were incorporated into the model, as the objective of the study is to evaluate natural channel–floodplain interactions within a geomorphologically controlled mountainous microcatchment. This modeling assumption is consistent with hazard-oriented flood simulations in comparable steep-terrain environments (Teng et al., 2017).

Flood intensity exhibits significant spatial variability, primarily influenced by topographic slope and rainfall intensity. Therefore, mapping flood hazard zones along the main river course is particularly critical for settlements located at river confluences or downstream basin areas (Tamiru & Dinka, 2021).

Manning's roughness coefficients were assigned using a land use–based approach derived from CORINE Land Cover data and supported by field observations within the microcatchment. Roughness values were selected according to established hydraulic references (Akan, 2006; Arcement & Schneider, 1989) and implemented as spatially distributed roughness polygons within the 2D HEC-RAS computational domain. The adopted Manning's n values ranged between 0.035 for the main gravel-bed channel and 0.10 for settlement areas, with intermediate values applied to agricultural and forested surfaces. To enhance model reliability, a sensitivity-based calibration was conducted against the documented 2020 Şehittepe flood event, testing roughness variations within the range of 0.03–0.07. This calibration procedure ensured that simulated water depths and hazard classifications were consistent with observed inundation extents, thereby strengthening the replicability and hydraulic robustness of the modeling framework.

Baseflow conditions were not explicitly incorporated into the model, as the primary objective was to simulate extreme flood scenarios under peak discharge conditions (Q100), where surface runoff dominates the hydrodynamic response. This assumption is consistent with event-based flood modeling approaches widely adopted in the literature (Peker et al., 2024). The flood hazard classification applied in the HEC-RAS simulations was based on a depth–velocity relationship (HR), allowing the categorization of hazard levels according to their potential impacts on human stability and infrastructure, in line with the widely used DEFRA methodology.

Furthermore, the adopted modeling framework is supported by recent studies integrating hydraulic modeling, GIS, and physically based parameterization for flood hazard assessment. Such approaches have been shown to significantly improve the accuracy and reliability of flood extent and hazard mapping by incorporating spatial variability and empirical parameter estimation (Demir & Keskin, 2020; Peker et al., 2024). In particular, the integration of spatially distributed roughness characterization and hydrodynamic modeling enhances the physical consistency and robustness of simulation outputs, thereby reinforcing the methodological reliability of the present study.

Model validation constitutes a critical step in ensuring the reliability and transferability of hydraulic simulations, particularly in complex mountainous terrains (Horritt & Bates, 2002; Bates et al., 2005).

In this study, the 2D HEC-RAS flood model was validated through spatial comparison between simulated inundation extents and documented flood footprints from the 2020 Şehittepe flood event. Observed flood boundaries were digitized from municipal records, field-based documentation, and post-event assessments.

The observed flood footprints of the 2020 Şehittepe event were reconstructed using a multi-source spatial documentation approach. Post-event flood boundaries were digitized in ArcGIS Pro by integrating georeferenced municipal damage reports, field-based GPS observations, and photographic records collected immediately after the flood. These sources were first converted into geospatial layers and visually interpreted to delineate maximum inundation limits. The resulting observed flood polygon was then compared with the

simulated inundation extent derived from the HEC-RAS 2D model. Spatial agreement between the two datasets was quantified using a GIS-based overlay analysis, where the overlap index was calculated as the ratio of intersecting area to the union of observed and modeled inundation extents.

A GIS-based overlay analysis was performed to quantify spatial agreement between modeled and observed flood extents. The spatial overlap ratio reached approximately 76%, indicating satisfactory performance for microcatchment-scale 2D hydraulic modeling in steep topographic settings. Similar agreement levels have been reported in comparable mountainous flood modeling studies (Teng et al., 2017; Costabile et al., 2009).

In addition to spatial validation, qualitative verification was supported by field observations of maximum flood depth marks and reported impact zones. This combined quantitative–qualitative validation framework enhances the robustness and replicability of the hydraulic modeling approach.

Following the development of a flood hazard classification scheme, a four-class flood risk map was generated for the microcatchment and incorporated into the study (Table 3). This spatially explicit risk mapping provides a robust framework for guiding risk-informed land use planning and enhancing the effectiveness of early warning and mitigation strategies.

Table 3. Flood hazard classification matrix (Apel et al., 2004; de Moel et al., 2009; DEFRA, 2006; WMO, 2009)

Hazard Value $\mathbf{HR = dx(v + 0,5)}$	**Flood Hazard Level**	**Risk Description**
<0,75	Low	Usually safe — shallow and/or slow water
0,75-1,25	Moderate	Dangerous for some (e.g., children)
1,25-2,5	Significant	Dangerous for most people
>2,5	Extreme	Dangerous for all — deep and fast flow

These outputs were integrated with land use data and exposure levels to delineate flood hazard zones (Z1–Z4) within the study area (Figure 5).

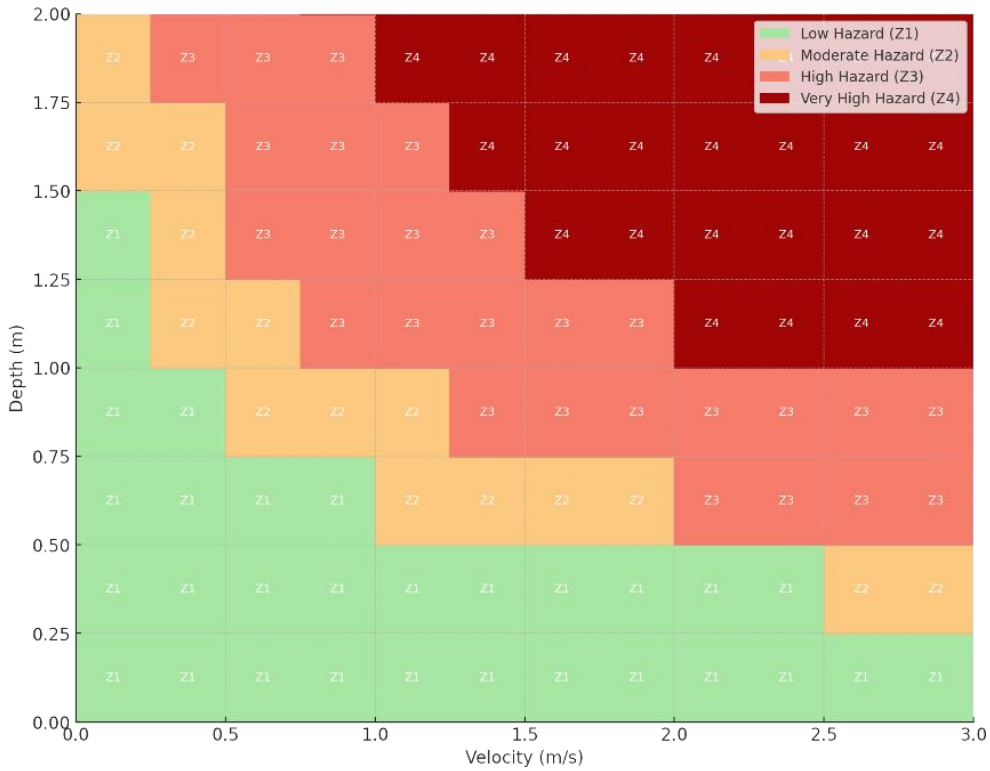


Figure 5. Flood hazard classification matrix

The methodological workflow adopted for flood simulation development is detailed in Figure 6.

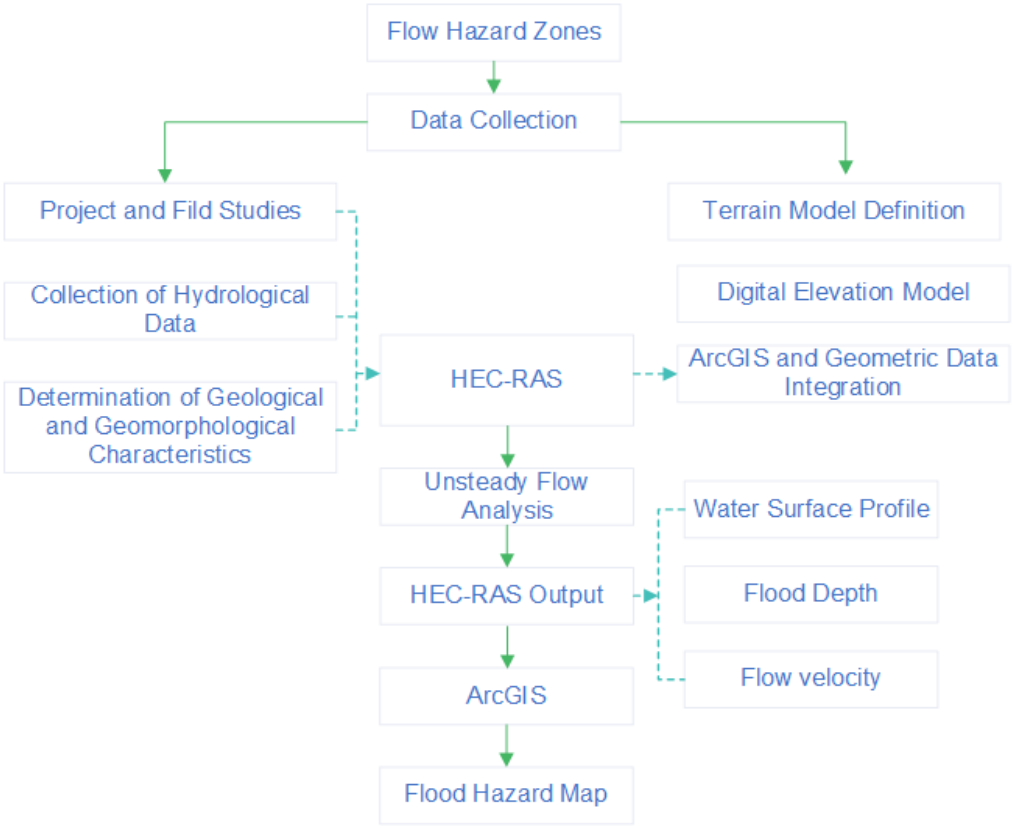


Figure 6. Methodological workflow for delineating flood hazard zones and simulating flood flow dynamics using the HEC-RAS model (Akkuş et al., 2023; Namara et al., 2022)

3. Results

3.1. Avalanche hazard assessments in Lediz microcatchment

Avalanche hazard assessment was conducted using the RAMMS (Rapid Mass Movement Simulation) model, considering the topographic and morphodynamic characteristics of the study area. The analysis integrated model outputs with slope, aspect, and elevation data derived from the Digital Elevation Model (DEM) within the ArcGIS Pro environment. The classification was based on a multi-parameter evaluation that simultaneously considered maximum flow velocity, dynamic pressure, and flow height parameters that collectively reflect the physical intensity of avalanche dynamics. The threshold values adopted for hazard classification followed internationally recognized standards (Bartelt et al., 2017; Margreth et al., 2017; Sovilla et al. 2018), delineating four risk levels: Low, Moderate, Significant, and Extreme. This approach enabled a hazard zonation framework that accounts not only for morphological conditions but also for the kinetic energy and impact pressure components of avalanche movement. (Figure 7).

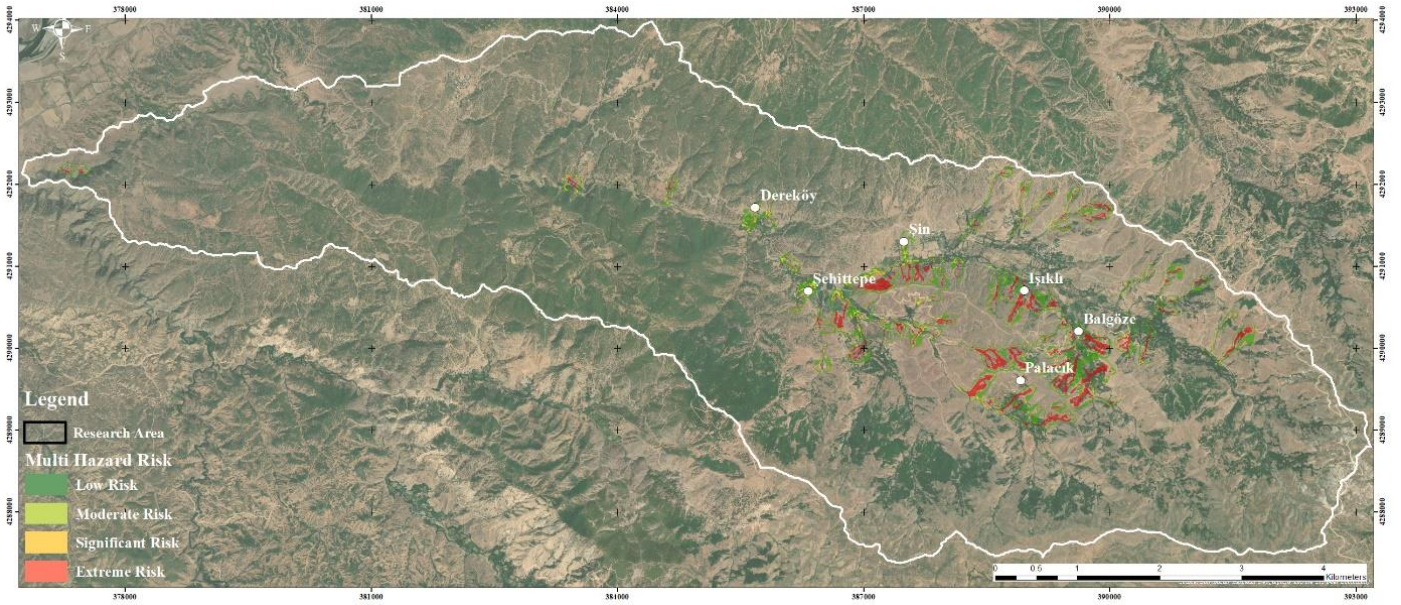


Figure 7. Spatial distribution of avalanche-prone zones and settlement areas within the microcatchment

The results indicate that high-slope and north-facing terrain units exhibit the most critical avalanche conditions, where flow velocity and dynamic pressure frequently exceed the identified hazard thresholds. These zones coincide with potential exposure of settlements, transportation corridors, and energy infrastructure. Such findings are consistent with the avalanche dynamics described by (Bartelt et al., 2017) and Sovilla et al., (2018), confirming that the integration of velocity, pressure, and flow height improves the physical realism and spatial accuracy of hazard mapping. Moreover, in accordance with Margreth et al. (2017), the adoption of a multi-parameter hazard framework significantly enhances the reliability of risk zonation by quantifying both avalanche initiation potential and impact intensity. Overall, this modeling strategy provides a scientifically robust basis for engineering design, spatial planning, and comprehensive risk management in mountainous regions.

The RAMMS simulations produced peak values of 30.6 m/s in flow velocity and 281.1 kPa in dynamic pressure, substantially exceeding the widely recognized destructive thresholds of 15 m/s and 100 kPa. The RAMMS simulations produced peak avalanche velocities of up to 30.6 m/s and dynamic pressures reaching 281 kPa. Although the simulated peak velocity of 30.6 m/s appears relatively high, it remains within the upper range reported for dense snow avalanches in steep and confined mountain terrain. Previous studies have documented avalanche velocities exceeding 30 m/s in narrow channelized slopes where terrain confinement significantly accelerates flow dynamics (Bartelt et al., 2017; Christen et al., 2010). In the Lediz Microcatchment, such peak values occur primarily within steep avalanche corridors where slope gradients and valley confinement amplify gravitational acceleration and channelized flow behavior. These terrain-controlled conditions promote localized increases in avalanche velocity and dynamic pressure, explaining the high simulated values observed in the model outputs. These extreme values indicate that certain sectors of the microcatchment fall well within the Extreme (Z4) hazard class, implying catastrophic structural impact potential rather than moderate damage scenarios. The concentration of such values in slope-confined corridors proximal to Dereköy and Şehittepe suggests localized terrain amplification effects.

The analysis revealed that agricultural lands and residential areas in the villages of Dereköy, Şehittepe, and Şin within the microcatchment are potentially exposed to avalanche hazards, primarily due to their proximity to steep slopes and established avalanche runout

corridors. Model simulations demonstrated that these settlements are located within or adjacent to dynamic flow zones where snow accumulation, slope gradient, and prevailing wind direction jointly enhance the probability of avalanche initiation. Likewise, the upper catchment assessment indicated that residential and agricultural areas in the Balgöze village center, as well as in the Işıklı and Palacık hamlets, are also susceptible to the compound effects of avalanche and flood processes. This spatial convergence of multiple geomorphic hazards highlights the complex hazard dynamics governing the basin and emphasizes the urgent need for the integration of structural mitigation measures and land-use planning strategies aimed at minimizing community exposure to high-intensity natural hazard events (Figure 8).

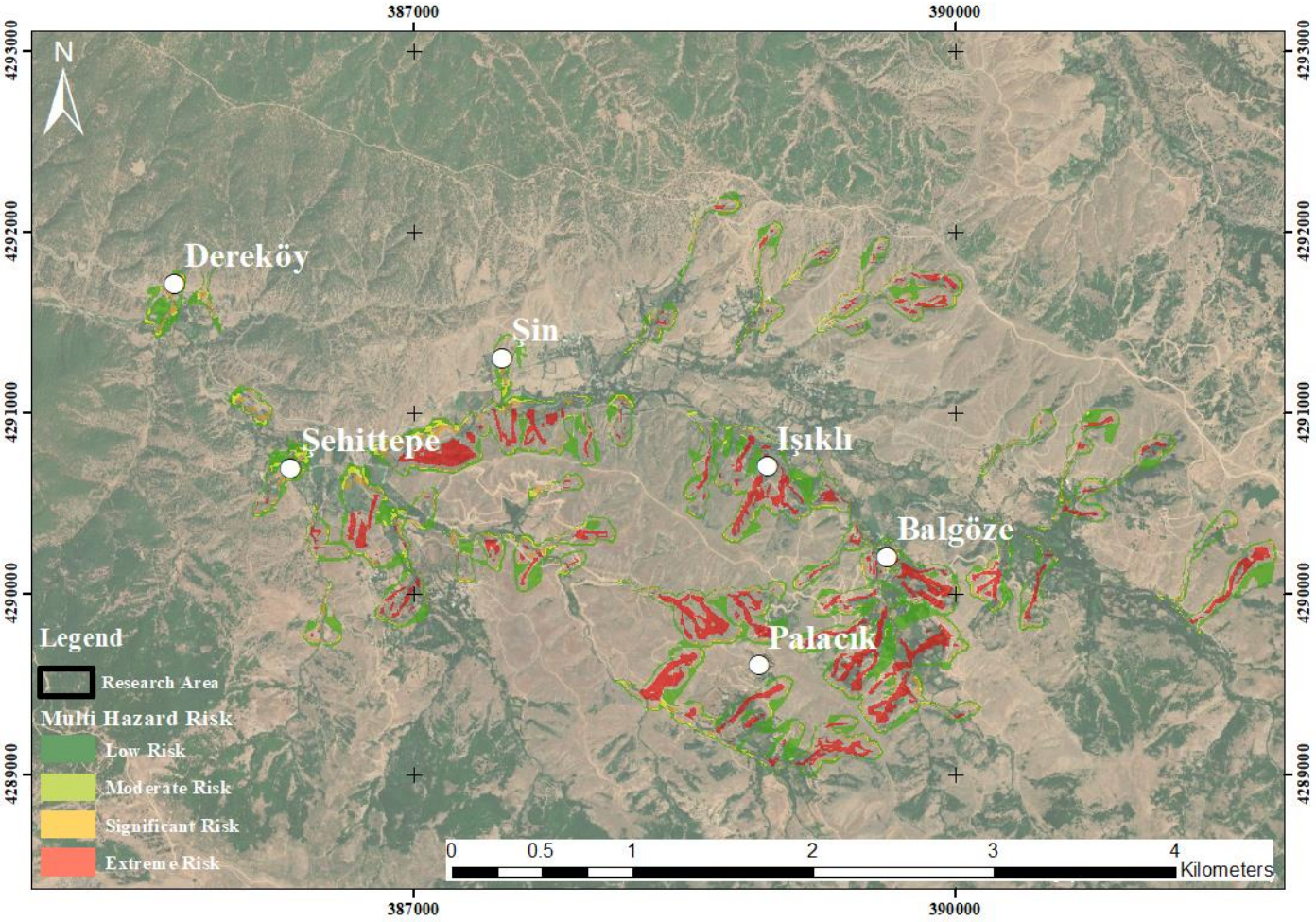


Figure 8. Spatial distribution of avalanche-prone zones and settlement areas in the microcatchment

3.2. Flood Hazard Assessment in the Lediz Microcatchment

The flood hazard assessment was conducted using the HEC-RAS (Hydrologic Engineering Center's River Analysis System) model to simulate maximum water depth, flow velocity, and inundation extent under peak discharge conditions. Model outputs were integrated into the ArcGIS Pro environment to delineate flood-prone zones and to examine their spatial relationship with existing land-use patterns. The analysis revealed that flood dynamics within the microcatchment are primarily confined to narrow stream channels and adjacent low-lying terraces, where flow velocities and inundation depths remain below critical thresholds. As a result, the flood hazard does not independently pose a significant threat to agricultural lands or residential zones within the study area. This finding indicates that, in isolation, fluvial processes exhibit limited geomorphic and infrastructural impact across the microcatchment. However, the hydrological pathways identified by the model hold particular importance when interacting with other slope-related processes (such as

avalanches or debris flows) since they may act as secondary accumulation or drainage corridors during extreme events. This interpretation is consistent with the observations of Gallina et al. (2016) and Kappes et al. (2012), who emphasized that single-process flood hazards in mountain environments often gain significance only when coupled with other rapid mass movement phenomena.

Overall, the HEC-RAS based analysis underscores the need to consider flood hazards within the microcatchment not as isolated threats, but as integral components of a compound hazard system shaping the hydromorphological dynamics of the Lediz microcatchment (Figure 9).

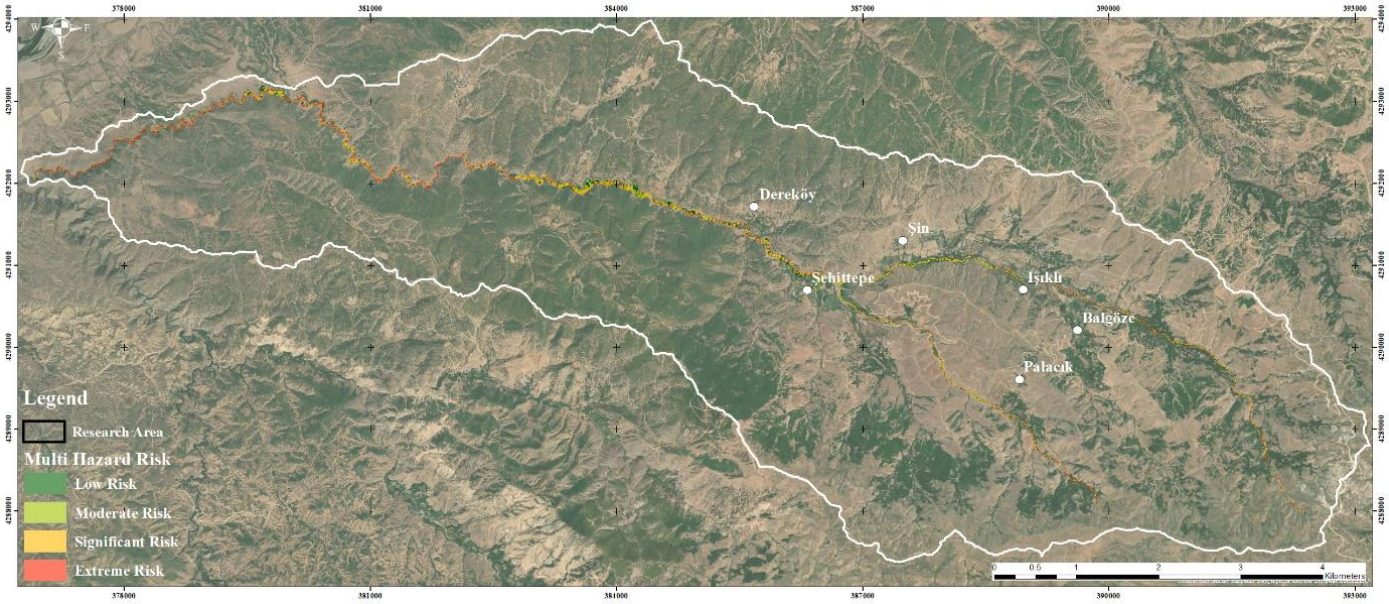


Figure 9. Spatial distribution of flood-prone areas simulated by the HEC-RAS model within the Lediz microcatchment

A high-resolution spatial analysis focusing on the settlement-scale zones within the Lediz microcatchment revealed the intricate interactions between topography, land use, and multi-hazard dynamics. The proximity of residential areas to steep slopes, confined valleys, and converging drainage lines indicates an elevated level of exposure, particularly to avalanche runout corridors and, to a lesser extent, seasonal flood channels. The detailed mapping conducted around the villages of Dereköy, Şehittepe, Şin, and Balgöze demonstrates that several residential clusters and agricultural terraces are in proximity to identified hazard boundaries (Figure 10). This spatial adjacency underscores the necessity for micro-scale hazard zoning and risk-sensitive settlement planning, especially in areas where built-up zones are expanding toward natural flow corridors. Furthermore, the results indicate that although flood processes alone exert limited geomorphic influence within the microcatchment, their spatial overlap with avalanche-prone terrain can significantly amplify hazard intensity during extreme precipitation or rapid snowmelt events. These findings highlight the importance of implementing integrated, site-specific risk mitigation strategies that consider the cumulative and nonlinear interactions of geomorphic processes at the settlement level.

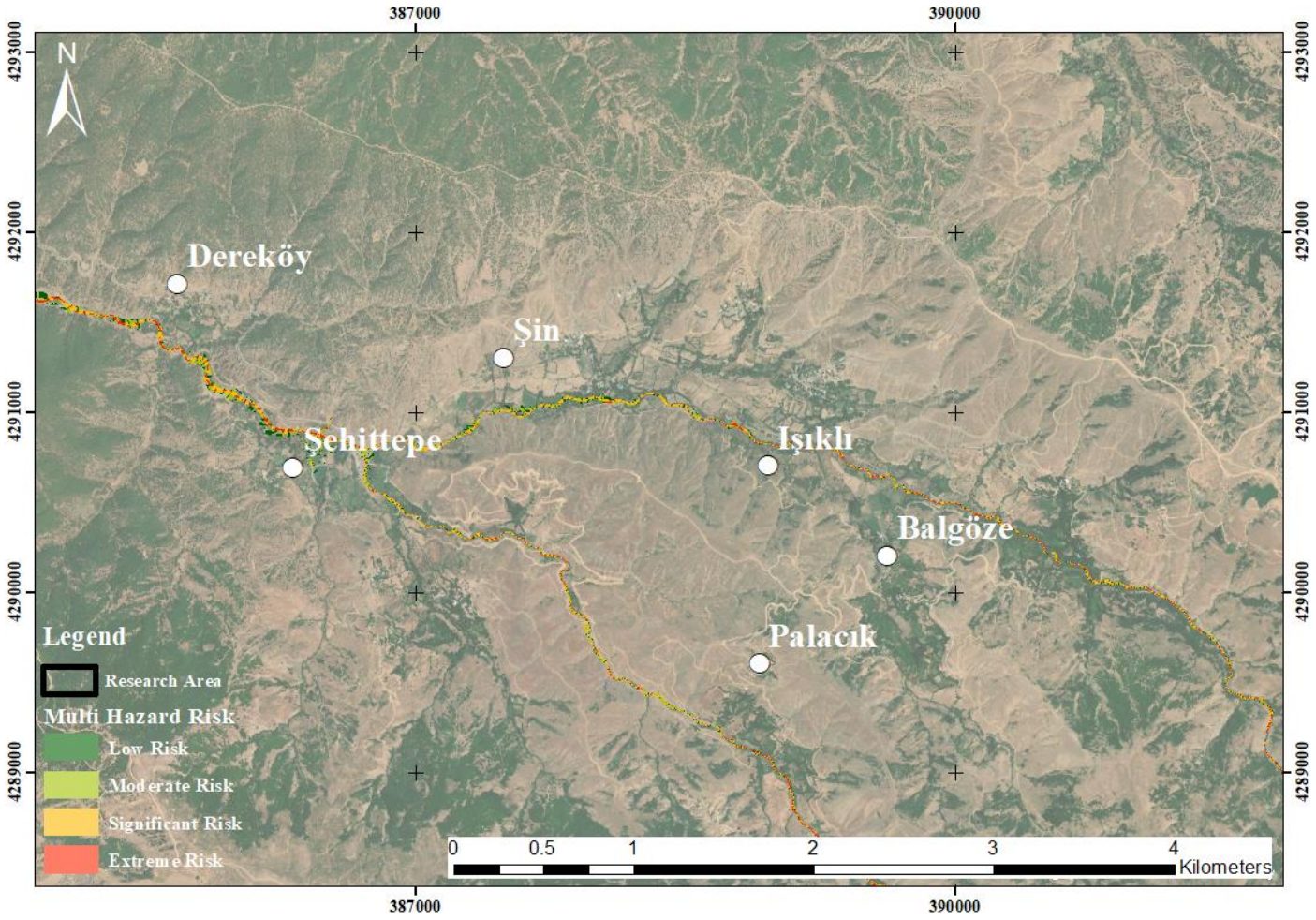


Figure 10. Spatial distribution of flood-prone areas simulated by the HEC-RAS model within the settlement areas in microcatchment

3.3. Compound avalanche–flood interaction and nonlinear risk amplification

Although the modeled peak discharge scenario indicates that independent flood intensities remain below critical structural damage thresholds within the microcatchment, this finding should not be interpreted as negligible flood risk. Under projected climate variability characterized by intensified rainfall events and rapid snowmelt episodes, peak discharges may substantially increase, potentially shifting currently moderate flood zones into destructive hazard classes. Therefore, flood dynamics should be regarded as conditionally critical processes whose risk significance depends on both climatic forcing and compound interaction mechanisms.

This phenomenon aligns with the multi-hazard amplification framework described by Gallina et al. (2016) and Kappes et al. (2012), wherein one process can significantly increase the destructive potential of another through spatial or temporal overlap. Similarly, (Argue et al., 2023) emphasized that in mountainous environments, snowpack accumulation and slope morphology exert strong control over flood regimes, producing nonlinear escalations of risk when gravitational and hydrological processes interact. Figure 11 and Figure 12 illustrates this compound effect, depicting the spatial convergence of avalanche and flood hazards where integrated processes result in the highest combined risk.

The convergence of Significant–Extreme avalanche zones (Z3–Z4) with flood hazard classes exceeding HR > 2.5 can be interpreted as compound hazard hotspots. In these sectors, dynamic snow loading and hydrodynamic forces may operate concurrently, producing nonlinear amplification of structural and socio-economic risk. These zones therefore represent priority intervention areas within the microcatchment, where cascading

interactions between gravitational and fluvial processes may significantly intensify overall hazard impact.

In addition to this spatial convergence, a potential hydro-dynamic interaction mechanism may involve temporary channel obstruction caused by avalanche debris accumulation. In steep and confined valley segments of the Lediz Microcatchment, dense snow masses and entrained materials could partially block stream channels, potentially forming short-lived debris dams. In such confined reaches, deposition thickness exceeding approximately 40–60% of the local bankfull channel depth may significantly reduce conveyance capacity and induce temporary backwater effects under peak discharge conditions. Such obstruction may therefore amplify upstream inundation beyond hydraulically modeled steady conveyance scenarios. Such blockage may induce localized backwater effects and secondary upstream inundation, thereby amplifying flood intensity beyond hydraulically modeled conditions. Although the present modeling framework treats avalanche and flood processes sequentially rather than through dynamic coupling, debris-induced channel obstruction represents a realistic amplification pathway under extreme snow loading conditions. Future research incorporating fully coupled hydro-gravitational simulations would provide deeper insight into such cascading process interactions.

Nevertheless, risk within the Lediz microcatchment cannot be adequately explained by physical hazard intensity alone. Socio-economic vulnerability significantly constrains post-disaster recovery capacity. Field data indicate that approximately 78% of the local population lacks formal social security coverage, while annual household income levels predominantly range between 1,000–2,000 USD. In settlements such as Balgöze and Işıklı, where high hazard exposure intersects with limited economic resilience, disaster impacts may translate into prolonged recovery cycles and structural displacement. Accordingly, risk should be interpreted as the interaction between modeled hazard intensity and constrained adaptive capacity. In this context, disaster risk within the Lediz Microcatchment can be conceptually framed as the functional interaction between physical hazard intensity (H) and socio-economic vulnerability (V), where limited adaptive capacity amplifies the consequences of even moderate hazard levels. Thus, spatial overlap alone does not define risk magnitude; rather, risk emerges from the coupling of dynamic hazard processes with constrained recovery potential.

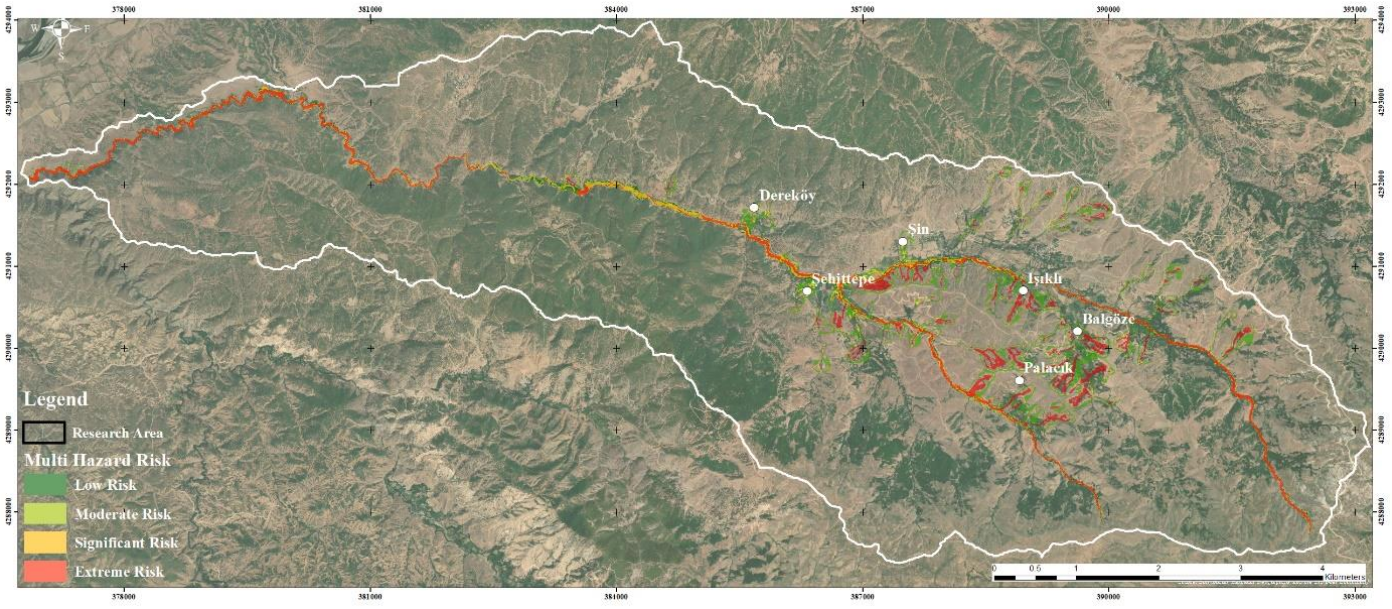


Figure 11. Integrated multi-hazard risk map of the Lediz microcatchment showing the spatial convergence of avalanche and flood hazard zones

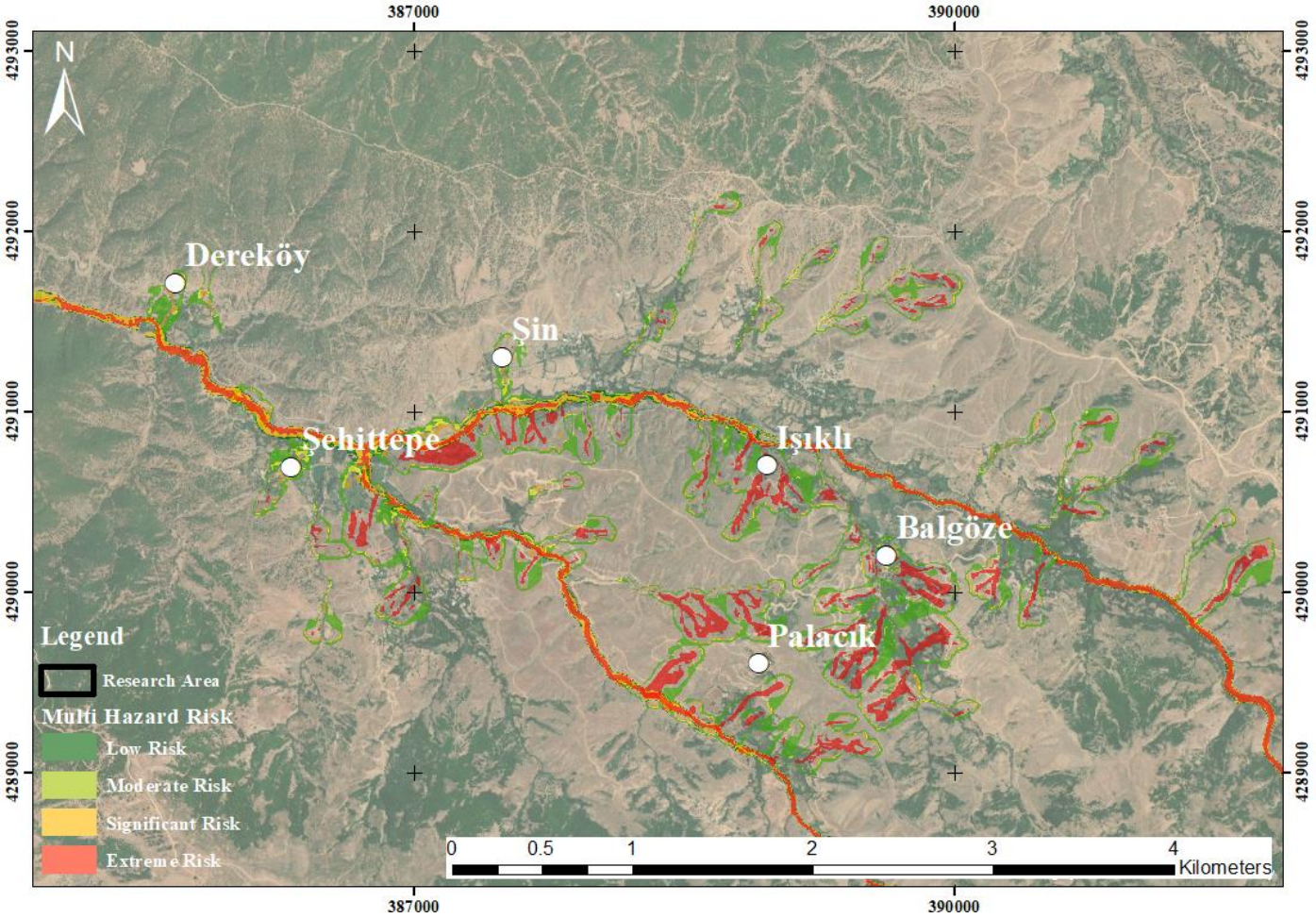


Figure 12. Integrated multi-hazard risk map of settlement areas in the Lediz microcatchment showing the spatial convergence of avalanche and flood hazard zones

4. Discussion

In the context of the Lediz microcatchment, these interactions demonstrate that although fluvial hazards are independently of limited structural impact under modeled peak discharge conditions, their coincidence with avalanche dynamics transforms them into a critical driver of compound disaster potential. Consequently, risk assessment in such environments must extend beyond single-hazard approaches to incorporate the synergistic and feedback-driven relationships among geomorphic processes as a prerequisite for effective, sustainable hazard management in mountain regions. This process-based interpretation demonstrates that multi-hazard risk in mountainous microcatchments is not additive but dynamically amplified through geomorphic-hydraulic feedback mechanisms.

These findings underscore the need for integrated risk management strategies in multi-hazard-prone rural landscapes.

Avalanche flow paths derived from RAMMS simulations in the Lediz Microcatchment were validated against field observations of avalanche events recorded by the Bingöl Provincial Disaster and Emergency Directorate (AFAD) in 2018 and 2021. A strong spatial correspondence was observed between model outputs (specifically maximum snow depth, flow velocity (>15 m/s), and dynamic pressure (>100 kPa)) with AFAD field data. Validation of the RAMMS and HEC-RAS simulations was conducted by comparing model outputs with documented historical hazard records. For avalanche events, spatial outlines provided by AFAD were cross-checked against the simulated runout zones. Flood simulations were compared with inundation areas reported in DSİ and municipal records. The degree of correspondence was measured as the proportion of overlapping areas, which indicated a 76% spatial match between observed and modeled hazard extents. In addition, qualitative

validation was obtained through feedback from local stakeholders, including residents and municipal staff, who confirmed that the simulated hazard zones were consistent with their experiences of past events. This combined approach provides both quantitative and qualitative support for the credibility of the modeling results. Notably, 76% of simulated avalanche paths overlapped with actual tracks, with deviations in snow depth limited to ±15 m. This level of accuracy aligns with previous studies demonstrating the reliability of RAMMS in mountainous environments (AFAD, 2021; Bartelt et al., 2012; Bühler et al., 2019).

To strengthen the validation results, quantitative outputs from the RAMMS simulations were visualized and compared against critical thresholds and field observations. The simulation yielded a maximum velocity of 30.6 m/s, a maximum flow height of 15.1 m, and a dynamic pressure of 281 kPa, with an overall released snow volume of approximately 842,752 m^3 (Figure 13).

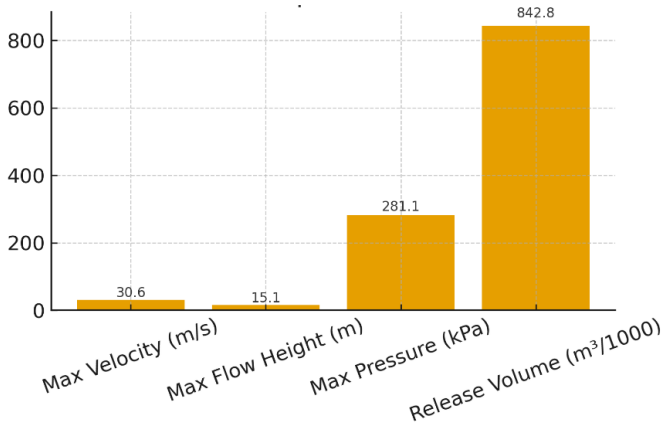


Figure 13. Maximum outputs of the RAMMS simulation for the Lediz microcatchment, showing flow velocity, flow height, dynamic pressure, and released snow volume

These values are well above the critical thresholds of 15 m/s and 100 kPa, which are commonly used in avalanche risk assessments to define destructive potential. Figure 14 further illustrates that the modelled parameters significantly exceeded these validation thresholds, supporting the interpretation that the simulated avalanche dynamics align with destructive events documented by AFAD in 2018 and 2021. Together with the ±15 m deviation in snow depth and the 76% spatial overlap between RAMMS outputs and AFAD-observed avalanche tracks, these results provide strong visual and quantitative evidence of model credibility.

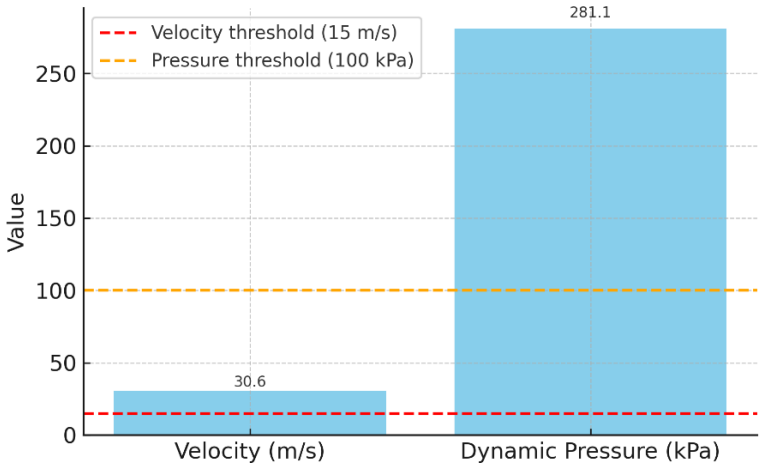


Figure 14. Comparison of RAMMS maximum velocity and dynamic pressure with validation thresholds of 15 m/s and 100 kPa, showing that simulated values substantially exceed critical limits

This study's multi-hazard assessment gains greater significance when viewed through the lens of socio-economic vulnerability. Surveys conducted in the Lediz and surrounding microcatchments revealed that 78% of households lack social security, 72.4% have an annual income of only 1,000–2,000 $, and the majority rely on agriculture and livestock as their primary sources of livelihood (Baydaş et al., 2018). Furthermore, 15% of respondents are illiterate and only 0.8% hold a university degree, indicating limited disaster awareness and adaptive capacity. As highlighted in the literature, risk is not solely determined by physical exposure, but also by socio-economic fragility, institutional capacity, and adaptive responses (Birkmann et al., 2017; Koks et al., 2019). Integrating these dimensions into physical modeling outputs would enable more comprehensive risk assessments and ensure that highly vulnerable communities are prioritized in disaster risk reduction strategies (Jaafari et al., 2024).

Sensitivity analyses were conducted by varying Voellmy friction parameters (dry Coulomb friction coefficient (μ) and turbulent friction parameter (ξ)) across 12 scenarios. Results indicated that higher μ values reduced flow distance and peak velocity, while lower ξ values significantly increased dynamic pressure (Christen et al., 2010; RAMMS, 2024). These findings highlight the critical role of surface roughness and snow rheology in avalanche hazard assessment.

Similarly, 2D HEC-RAS flood simulations were validated using historical data and local stakeholder observations. The 2020 flood in Şehittepe village served as a key reference event. The model accurately identified areas where the flood hazard rating (HR) exceeded 2.5, consistent with observed inundation extents. Sensitivity tests on Manning's roughness coefficient (0.03–0.07), peak hydrograph discharge (±10%), and grid resolution (5–10 m) revealed that variations in Manning's coefficient could affect water depth by up to 12%, while lower grid resolutions led to a 17% underestimation of hazard classification (AL-Hussein et al., 2022; Leandro & Martins, 2016). These results underscore the importance of high-resolution topographic data and precise calibration in flood hazard modeling.

The combined application of RAMMS and HEC-RAS demonstrated that avalanche and flood hazards in the Lediz Microcatchment can occur simultaneously or act as triggers for one another. Simulations revealed that high to very high avalanche hazard zones are concentrated in steep, snow-prone areas, while critical flood hazards are prominent along valley corridors and near settlements (Figures 5–7). This spatial overlap suggests a substantial potential for compound hazard interactions in mountainous catchments (Gariano & Guzzetti, 2016; Lee et al., 2024).

Scenarios with RAMMS outputs exceeding 15 m/s in velocity and 100 kPa in pressure indicate a high risk of structural damage and casualties in settlements such as Dereköy and Şehittepe. These thresholds have been identified as critical indicators of destructive avalanche potential (Bartelt et al., 2017). Overlapping avalanche and flood hazard zones in the Lediz Microcatchment can be characterized as "compound hazard hotspots," which are critical not only from a physical risk perspective but also in terms of social and economic vulnerability (Koks et al., 2019) However, the absence of detailed socio-economic data limits the ability to fully assess community resilience and preparedness (Birkmann et al., 2017; Birkmann et al., 2023). The identification of zones exceeding destructive avalanche thresholds and overlapping with high flood hazard ratings further reinforces the necessity of compound-risk-oriented land-use regulation and micro-scale settlement planning.

Similarly, flood zones with HR values >2.5 identified through HEC-RAS simulations pose significant risks to agricultural lands (Apel et al., 2004, 2009; de Moel et al., 2009). These findings reinforce that independent hazard assessments are insufficient for effective risk management in small-scale catchment planning. As Kappes et al., (2012) and (Wang et al., 2020) emphasize, multi-hazard processes require integrated analysis due to their dynamic and interactive nature. The spatial overlap of avalanche and flood hazard zones observed in this study further supports this integrated approach.

While the presented results demonstrate strong spatial correspondence between simulated and observed hazard zones, a deeper interpretation is required when considering model uncertainties and inherent limitations. Avalanche simulations are highly sensitive to Voellmy friction parameters and release zone delineation, whereas flood simulations depend on Manning's coefficient and the resolution of digital elevation models. Such sensitivities indicate that identified compound hotspots should be interpreted as probabilistic rather than deterministic outcomes. The sensitivity results demonstrate that small variations in friction, roughness, or grid resolution can lead to measurable changes in hazard extent and intensity. Therefore, the presented risk zones should not be interpreted as fixed boundaries but rather as confidence-based spatial estimates. Consequently, identified compound hazard hotspots should be interpreted as high-probability zones rather than deterministic boundaries. The presented maps represent confidence-based spatial estimates derived from calibrated physical modeling and sensitivity testing. This probabilistic perspective is essential for avoiding overconfidence in fixed zoning thresholds, particularly in steep, confined valley systems where small parameter variations can induce nonlinear spatial responses. This probabilistic interpretation is particularly important in narrow valley systems, where DEM resolution strongly influences hydraulic routing and avalanche channelization. In particular, the 17% underestimation observed under lower grid resolutions highlights the susceptibility of flood hazard classification to DEM smoothing effects in confined valley geometries. Moreover, the current framework assesses hazards sequentially and evaluates their spatial overlap, but does not fully capture cascading or temporally correlated processes (such as avalanche-induced flooding) which are increasingly recognized as critical in mountain environments (Gariano & Guzzetti, 2016; Jaafari et al., 2024; Sharma et al., 2023). Therefore, the presented compound hotspots should be interpreted as spatially co-located risk potentials rather than dynamically simulated cascade events. Future research should therefore integrate causal modeling approaches, including Bayesian networks, system dynamics, or scenario-based probabilistic chains, to account for multi-temporal interactions and cascading effects (Nadim et al., 2014; Terzi et al., 2019). Embedding these advanced methods would provide a more robust analytical foundation, moving the study beyond descriptive mapping toward a critical interpretation of systemic multi-hazard risks.

There is growing recognition in the literature of the need to couple nature-based solutions with risk-informed management strategies in multi-hazard contexts (Rahmati et al., 2016, 2019; Van Westen & Greiving, 2017). The joint application of physically based models such as RAMMS and HEC-RAS enables both detailed risk zone mapping and informed prioritization of mitigation actions. Furthermore, such models facilitate the development of synchronized hazard scenarios, enhancing decision-making capacity (Marzocchi et al., 2009).

The Lediz Microcatchment (characterized by complex topography, an average of 76 snow-covered days, and 831 mm annual precipitation) provides a representative setting for multi-hazard modeling (Baydaş et al., 2018; OGM, 2013). Land-use patterns (agriculture–forest–settlement) further influence local risk dynamics, highlighting the need for spatially targeted planning. The strong correlation between avalanche release areas and slopes >30°, along with concave landforms, supports model accuracy and sensitivity (Maggioni et al., 2002; Maggioni & Gruber, 2003).

The integrated framework presented here offers a practical example of multi-hazard-sensitive landscape planning. The combined use of RAMMS and HEC-RAS supports not only pre-disaster risk assessment but also strategic post-disaster recovery planning (Jaafari et al., 2024; Tilloy et al., 2019). As climate change drives increases in rapid warming events, irregular precipitation, and extreme snowfall, the likelihood of compound avalanche–flood events will grow. Lee et al. (2024) and Zscheischler et al. (2018) term such phenomena "compound events" and argue that conventional hazard frameworks are inadequate to address them. Our findings support this view, underscoring the need for scenario-based multi-risk analyses in disaster planning. The clear exposure of settlements and agricultural

lands to both avalanche and flood hazards further highlights the necessity of integrating nature-based solutions in managing vulnerable landscapes. Such approaches not only mitigate disaster risks but also enhance ecosystem services and strengthen socio-ecological resilience (Kabisch et al., 2017).

This study contributes to the development of resilient infrastructure and settlement strategies for mountain communities. Its key innovation lies in the spatial overlap analysis achieved through the integrated use of RAMMS and HEC-RAS outputs. This approach enables the incorporation of risk assessment and prioritization within spatial planning processes. The literature clearly demonstrates that such integrated models enhance decision-support systems, particularly in hazard-prone mountainous regions (Carpignano et al., 2009; Sharma & Miyazaki, 2019).

Multi-hazard modeling is essential for understanding the interactions between hazards such as avalanches and floods in mountainous environments. The integrated application of RAMMS and HEC-RAS in this study effectively identified areas of spatial overlap between these hazards in the Lediz Microcatchment. However, a comprehensive understanding of multi-hazard dynamics requires the integration of social, temporal, and systemic complexities alongside physical modeling (Gill & Malamud, 2014; Kappes et al., 2012).

In this study, hazards were modeled separately and then analyzed for spatial overlap. Yet, as highlighted in recent literature (Lee et al., 2024; Tilloy et al., 2019; Zscheischler et al., 2018), critical components of multi-risk analysis include simultaneity, causal chains, and compound event dynamics. In particular, the temporal correlations between avalanche and flood events (e.g., rapid surface runoff following snowmelt) should be analyzed not only in terms of concurrent exposure but also through trigger–response relationships. While such interactions were conceptually addressed in this study, quantitative analyses of causality (e.g., regression analysis, conditional probability modeling) remain a task for future work.

While the primary modeling framework focuses on physical hazard intensity, the present study contextualizes results using socio-economic indicators to interpret recovery capacity and spatial vulnerability patterns. The impacts of multi-hazard systems extend beyond physical damage; factors such as livelihoods, transportation connectivity, and recovery rates are critical in rural areas (Birkmann et al., 2017; Birkmann et al., 2023; Koks et al., 2019). Future studies should integrate physical hazard modeling with spatially explicit social vulnerability indices to support more equitable and effective intervention strategies.

Finally, while the composite risk maps produced in this study represent an important first step, they should be supplemented with scenario-based decision-support tools. As Marzocchi et al. (2009) and Van Westen & Greiving, (2017) emphasize, synchronized "what-if" multi-hazard scenarios can provide decision-makers with insights into potential outcomes under varying conditions.

In conclusion, while this study makes an important contribution to the multi-risk framework, there remains significant potential to strengthen multi-hazard management through the systematic integration of dynamic, cascading, and socially sensitive components.

5. Conclusions

This study demonstrates that natural hazards such as avalanches and floods, whose frequency and severity are increasing under the influence of climate change, have a significant potential to develop concurrently and interactively, particularly in mountainous microcatchments. The integrated analyses conducted in the Lediz Microcatchment using RAMMS and HEC-RAS models clearly reveal that disaster risks must be assessed not only through physical parameters but also by considering their socio-economic impacts. The findings identified numerous areas where avalanche and flood risks spatially overlap; designating these areas as compound hazard hotspots is critical for prioritizing disaster planning and response strategies. Specifically, settlements such as Dereköy, Şehittepe, Şin, Balgöze, Işıklı, and Palacık were found to be directly exposed to zones characterized by high

dynamic pressure (>100 kPa), high flow velocity (>15 m/s), and elevated flood hazard ratings (HR > 2.5). This situation poses threats not only to life and property but also to the long-term sustainability of local infrastructure.

Accordingly, the produced hazard maps should not be interpreted solely as spatial representations of physical danger, but rather as decision-support instruments for local governance and disaster risk management. By identifying zones of compound hazard exposure combined with socio-economic fragility, the framework enables evidence-based prioritization of budget allocation, infrastructure reinforcement, emergency logistics planning, and, where necessary, relocation strategies. This integrated perspective enhances the operational applicability of the study and supports strategic planning in hazard-prone rural landscapes.

The study further confirms the necessity of analyzing disaster risks as components of a dynamic system rather than in isolation. The combined use of physically based models like RAMMS and HEC-RAS facilitates the development of scenario-based early warning systems and enables more precise design of pre- and post-disaster response plans. In this context, synchronizing model outputs with spatial decision-support systems can provide a critical data source for capacity-building processes within local governments. Integrating model outputs with disaster management regulations and land-use planning is particularly essential for reducing risks in vulnerable mountainous landscapes.

Moreover, the study highlights the impacts of disaster risks on rural development and demographic sustainability. The overlap of high-risk zones with agricultural lands and settlements threatens the livelihoods of rural populations and may contribute to increased rural-to-urban migration. Therefore, disaster risk reduction policies should not focus solely on engineering solutions but also address the need for social support mechanisms that improve quality of life in rural areas. Planning strategies that promote in-situ development and incorporate nature-based solutions (e.g., flood retention areas, avalanche dams, green buffer zones) are valuable tools for mitigating migration pressures and enhancing rural resilience. Additionally, integrating hazard maps with socio-economic vulnerability data can help to make regional inequalities more visible and support the formulation of more equitable intervention priorities.

In addition to the physical modeling results, it is evident that socio-economic vulnerabilities play a decisive role in shaping disaster risk outcomes. Low-income levels, lack of social security, limited education, and livelihood dependence on agriculture and livestock restrict community resilience in the Lediz microcatchment (Baydaş et al., 2018). Future studies should therefore integrate these indicators with hazard models to deliver more holistic and actionable multi-risk management strategies (Birkmann et al., 2017; Jaafari et al., 2024).

The integrated modeling framework developed for the Lediz Microcatchment offers a scalable and adaptable approach for addressing compound hazard scenarios driven by climate change. This framework may serve as a model not only for mountainous catchments in Türkiye but also for other regions worldwide with similar geo-climatic conditions. Future research should further strengthen the interdisciplinary perspective by more explicitly linking hazard dynamics with local socio-ecological systems and by prioritizing resilience-based approaches that actively engage local communities.

Acknowledgments: The authors gratefully acknowledge the WSL Institute for Snow and Avalanche Research SLF for providing an academic license of the RAMMS::AVALANCHE simulation software. This support significantly contributed to the development and execution of the avalanche modeling framework presented in this study.

Author Contributions:

A. Meral: Conceptualization, Methodology, Software, Formal analysis, Investigation, Data curation, Visualization, Writing-original draft preparation.

E. Yıldız: Methodology, Software, Validation, Formal analysis, Investigation, Writing-review & editing.

AI Contribution Statement: No artificial intelligence (AI) tools were used in the preparation of this manuscript. All work was conducted entirely by the authors.

Funding: This study received no external funding.

Research and publication ethics statement: In the study, the authors declare that there is no violation of research and publication ethics and that the study does not require ethics committee approval.

Conflicts of Interest: The authors declare no conflicts of interest.

Data Availability: The data presented in this study are available on request from the corresponding author.

References

Abatzoglou, J. T., & Kolden, C. A. (2013). Relationships between climate and macroscale area burned in the western United States. *International Journal of Wildland Fire*, 22(7), 1003. https://doi.org/10.1071/WF13019

Ackerman, C. T., Fleming, M. J., & Brunner, G. W. (2008). Hydrologic and hydraulic models for performing dam break studies. *World Environmental and Water Resources Congress 2008*, 1–11. https://doi.org/10.1061/40976(316)285

AFAD. (2021). *[Bingöl] il afet risk azaltma planı*. Afet ve Acil Durum Yönetimi Başkanlığı.

Akan, O. (2006). Open channel hydraulics. Elsevier Publishing.

Akkuş, H., Yıldız, E., & Bulut, İ. (2023). HEC-RAS 2B Modeli Kullanılarak Yazılıkaya Deresi (Nallıhan Ankara) Sel Tehlike Haritalarının Hazırlanması ve Sel Kontrol Yapısının Etkinliği. *Jeoloji Mühendisliği Dergisi*, 47(1), 29–46. https://doi.org/10.24232/jmd.1268945

AL-Hussein, A. A. M., Khan, S., Ncibi, K., Hamdi, N., & Hamed, Y. (2022). Flood analysis using HEC-RAS and HEC-HMS: A case study of Khazir River (Middle East—Northern Iraq). *Water*, 14(22), 3779. https://doi.org/10.3390/w14223779

Amiri, M. J., & Eslamian, S. S. (2010). Investigation of Climate Change in Iran. *Journal of Environmental Science and Technology*, 3(4), 208–216. https://doi.org/10.3923/jest.2010.208.216

Apel, H., Aronica, G. T., Kreibich, H., & Thieken, A. H. (2009). Flood risk analyses—how detailed do we need to be? *Natural Hazards*, 49(1), 79–98. https://doi.org/10.1007/s11069-008-9277-8

Apel, H., Thieken, A. H., Merz, B., & Blöschl, G. (2004). Flood risk assessment and associated uncertainty. *Natural Hazards and Earth System Sciences*, 4(2), 295–308. https://doi.org/10.5194/nhess-4-295-2004

Arcement, G. J., & Schneider, V. R. (1989). Guide for selecting manning's roughness coefficients for natural channels and flood plains. *United States Government Printing Office*.

Argue, C., Jones, A., Gauthier, D., & Strouth, A. (2023). A common approach to multi-hazard risk assessment for avalanche and other slope hazards. *International Snow Science Workshop*, 773–779.

Ballesteros-Cánovas, J. A., Trappmann, D., Madrigal-González, J., Eckert, N., & Stoffel, M. (2018). Climate warming enhances snow avalanche risk in the Western Himalayas. *Proceedings of the National Academy of Sciences*, 115(13), 3410–3415. https://doi.org/10.1073/pnas.1716913115

Barbolini, M., Pagliardi, M., Ferro, F., & Corradeghini, P. (2011). Avalanche hazard mapping over large undocumented areas. *Natural Hazards*, 56(2), 451–464. https://doi.org/10.1007/s11069-009-9434-8

Barredo, J. I. (2007). Major flood disasters in Europe: 1950–2005. *Natural Hazards*, 42(1), 125–148. https://doi.org/10.1007/s11069-006-9065-2

Bartelt, P., Bühler, Y., Buser, O., Christen, M., & Meier, L. (2012). Modeling mass-dependent flow regime transitions to predict the stopping and depositional behavior of snow avalanches. *Journal of Geophysical Research: Earth Surface*, 117(F1). https://doi.org/10.1029/2010JF001957

Bartelt, P., Bühler, Y., Christen, M., Deubelbeiss, Y., Salz, M., Schneider, M., & Schumacher, L. (2017). RAMMS: Avalanche user manual. *Swiss Federal Institute of Technology.*

Bates, P. D., Pappenberger, F., & Romanowicz, R. J. (2005). Uncertainty in flood inundation modelling. *In Applied uncertainty analysis for flood risk management.*

Baydaş, A., Demirkıran, A., & Bilinmiş, M. M. (2018). Murat Nehri Rehabilitasyon projelerinden yöre halkının memnuniyet düzeyinin belirlenmesi: Bingöl (Lediz, Vahkin-Çanakçı, Göynük Çayı ve Çapakçur Mikrohavzaları) örneği. *Journal of Emerging Economies And Policy*, 3(1), 31–57.

Bell, R., & Glade, T. (2004). Multi-hazard analysis in natural risk assessments. *WIT Transaction on Ecology and the Environment*, 1(10), 197–206.

Bharath, A., Shivapur, A. V., & Hiremath, C. G. (2021). Dam break flood routing and inundation mapping using HEC-RAS and HEC-GeoRAS. *In Water Resources Management and Reservoir Operation* (pp. 129–137). https://doi.org/10.1007/978-3-030-79400-2_11

Birkmann, J. E., Liwenga, R., Pandey, E., Boyd, R., Djalante, F., Gemenne, W., Leal Filho, P. F., Stringer, L., & Wrathall, D. (2023). Poverty, Livelihoods and Sustainable Development. *In Climate Change 2022 – Impacts*, Adaptation and Vulnerability (pp. 1171–1284). Cambridge University Press. https://doi.org/10.1017/9781009325844.010

Birkmann, J., Sorg, L., & Welle, T. (2017). Disaster Vulnerability. In The Palgrave Handbook of Unconventional Risk Transfer (pp. 329–356). *Springer International Publishing*. https://doi.org/10.1007/978-3-319-59297-8_11

Brunner, G. W. (1995). HEC-RAS river analysis systems, hydraulic reference manual. *U.S. Army Corps of Engineers*.

Bühler, Y., Hafner, E. D., Zweifel, B., Zesiger, M., & Heisig, H. (2019). Where are the avalanches? Rapid SPOT6 satellite data acquisition to map an extreme avalanche period over the Swiss Alps. *The Cryosphere*, 13(12), 3225–3238. https://doi.org/10.5194/tc-13-3225-2019

Bulut, İ., Yüksel, A., Yıldız, E., Meral, A., Kolak, M. N., Kocademir, D., Akkuş, H., Mohabbi, M., & Varolgüneş, S. (2024). Türkiye'de çığ kontrol projelerinin hazırlanma süreçleri: Bingöl ili Adaklı ilçesi Aktaş köyü örneği. *Bingöl Üniversitesi Teknik Bilimler Dergisi*, 5(2), 13–27.

Bütün, L., & Koçyiğit, Ö. (2019). RAMMS programı ile simülasyon çalışması: Bozdağ örneğinde çığ tekerrür periyodunun sonuçlara etkisi. *International Science and Engineering Application Symposium on Hazards*, 169–173.

Carpignano, A., Golia, E., Di Mauro, C., Bouchon, S., & Nordvik, J. P. (2009). A methodological approach for the definition of multi-risk maps at regional level: first application. *Journal of Risk Research*, 12(3–4), 513–534. https://doi.org/10.1080/13669870903050269

Chow, V. T. (1959). *Open-channel hydraulics*. McGraw-Hill.

Christen, M., Kowalski, J., & Bartelt, P. (2010). RAMMS: Numerical simulation of dense snow avalanches in three-dimensional terrain. *Cold Regions Science and Technology*, 63(1–2), 1–14. https://doi.org/10.1016/j.coldregions.2010.04.005

Corona, C., & Stoffel, M. (2017). Snow and ice avalanches. *In International Encyclopedia of Geography* (pp. 1–7). Wiley. https://doi.org/10.1002/9781118786352.wbieg1123

Costabile, P., Costanzo, C., & Macchione, F. (2009). Two-dimensional numerical models for overland flow simulations. In *WIT Transactions on ecology and the environment*, WIT Press.

Cunge, J. A., Holly, F. M., & Verwey, A. (1980). *Practical aspects of computational river hydraulics*. Pitman.

de Moel, H., van Alphen, J., & Aerts, J. C. J. H. (2009). Flood maps in Europe – methods, availability and use. *Natural Hazards and Earth System Sciences*, 9(2), 289–301. https://doi.org/10.5194/nhess-9-289-2009

DEFRA. (2006). Flood risk to people/Phase 2.

Demir, E. (2018). Çığ hareketinin sayısal model ile incelenmesi; Bozdağ uygulaması [Doktora]. Gazi Üniversitesi.

Demir, V., & Keskin, A. Ü. (2019). Manning pürüzlülük katsayısının Cowan Yöntemi ve uzaktan algılama yardımıyla belirlenmesi. *Gazi Mühendislik Bilimleri Dergisi*, 5(2), 167-177.

Demir, V., Keskin, A. Ü. (2020). Obtaining the manning roughness with terrestrial-remote sensing technique and flood modeling using FLO-2D: A case study Samsun from Turkey. *Geofizika*, 37, 131-155.

Demircan, M., Gürkan, H., Eskioğlu, O., Arabacı, H., & Coşkun, M. (2017). Climate change projections for Turkey: Three models and two scenarios. *Turkish Journal of Water Science and Management*, 1(1), 22–43. https://doi.org/10.31807/tjwsm.297183

Dillon, J., & Hammonds, K. (2021). Brief communication: Initializing RAMMS with high resolution LIDAR data for avalanche simulations. In Preprint. https://doi.org/10.5194/tc-2020-368

Duvvuri, S., & Narasimhan, B. (2013). Flood inundation mapping of Thamiraparani River Basin using HEC-Geo RAS and SWAT. *International Journal of Engineering Research & Technology*, 2(7), 1408–1420.

Ebi, K. L. (2025). Understanding the risks of compound climate events and cascading risks. *Dialogues on Climate Change*, 2(1), 33–37. https://doi.org/10.1177/29768659241304857

Eskandari, S., & Chuvieco, E. (2015). Fire danger assessment in Iran based on geospatial information. *International Journal of Applied Earth Observation and Geoinformation*, 42, 57–64. https://doi.org/10.1016/j.jag.2015.05.006

Fuchs, S., Keiler, M., & Zischg, A. (2015). A spatiotemporal multi-hazard exposure assessment based on property data. *Natural Hazards* and Earth System Sciences, 15(9), 2127–2142. https://doi.org/10.5194/nhess-15-2127-2015

Gallina, V., Torresan, S., Critto, A., Sperotto, A., Glade, T., & Marcomini, A. (2016). A review of multi-risk methodologies for natural hazards: Consequences and challenges for a climate change impact assessment. *Journal of Environmental Management*, 168, 123–132. https://doi.org/10.1016/j.jenvman.2015.11.011

Gariano, S. L., & Guzzetti, F. (2016). Landslides in a changing climate. *Earth-Science Reviews*, 162, 227–252. https://doi.org/10.1016/j.earscirev.2016.08.011

Gayen, A., & Pourghasemi, H. R. (2019). Spatial modeling of gully erosion. *In Spatial Modeling in GIS and R for Earth and Environmental Sciences* (pp. 653–669). Elsevier. https://doi.org/10.1016/B978-0-12-815226-3.00030-2

Gigović, L., Pourghasemi, H. R., Drobnjak, S., & Bai, S. (2019). Testing a new ensemble model based on SVM and random forest in forest fire susceptibility assessment and its mapping in Serbia's Tara National Park. *Forests*, 10(5), 408. https://doi.org/10.3390/f10050408

Gill, J. C., & Malamud, B. D. (2014). Reviewing and visualizing the interactions of natural hazards. *Reviews of Geophysics*, 52(4), 680–722. https://doi.org/10.1002/2013RG000445

Gruber, U., & Bartelt, P. (2007). Snow avalanche hazard modelling of large areas using shallow water numerical methods and GIS. *Environmental Modelling & Software*, 22(10), 1472–1481. https://doi.org/10.1016/j.envsoft.2007.01.001

Haigh, M. J., Rawat, J. S., Rawat, M. S., Bartarya, S. K., & Rai, S. P. (1995). Interactions between forest and landslide activity along new highways in the Kumaun Himalaya. *Forest Ecology and Management*, 78(1–3), 173–189. https://doi.org/10.1016/0378-1127(95)03584-5

Hand, W. H., Fox, N. I., & Collier, C. G. (2004). A study of twentieth-century extreme rainfall events in the United Kingdom with implications for forecasting. *Meteorological Applications*, 11(1), 15–31. https://doi.org/10.1017/S1350482703001117

Horritt, M. S., & Bates, P. D. (2002). Evaluation of 1D and 2D numerical models for predicting river flood inundation. *Journal of Hydrology*, 1(4), 87–99.

Jaafari, A., Mafi-Gholami, D., & Yousefi, S. (2024). A spatiotemporal analysis using expert-weighted indicators for assessing social resilience to natural hazards. *Sustainable Cities and Society*, 100, 105051. https://doi.org/10.1016/j.scs.2023.105051

Kabisch, N., Korn, H., Stadler, J., & Bonn, A. (2017). Nature-Based Solutions to Climate Change Adaptation in Urban Areas. *Springer International Publishing*. https://doi.org/10.1007/978-3-319-56091-5

Kappes, M. S., Keiler, M., von Elverfeldt, K., & Glade, T. (2012). Challenges of analyzing multi-hazard risk: a review. *Natural Hazards*, 64(2), 1925–1958. https://doi.org/10.1007/s11069-012-0294-2

Koçyiğit, Ö., Tekin, E., & Arslan, G. (2016). Avalanche research studies at Bozdağ. *Disaster Science and Engineering*, 2(2), 40–45.

Koks, E. E., Rozenberg, J., Zorn, C., Tariverdi, M., Vousdoukas, M., Fraser, S. A., Hall, J. W., & Hallegatte, S. (2019). A global multi-hazard risk analysis of road and railway infrastructure assets. *Nature Communications*, 10(1), 2677. https://doi.org/10.1038/s41467-019-10442-3

Lamichhane, N., & Sharma, S. (2018). Effect of input data in hydraulic modeling for flood warning systems. *Hydrological Sciences Journal*, 63(6), 938–956. https://doi.org/10.1080/02626667.2018.1464166

Le Page, Y., Pereira, J. M. C., Trigo, R., da Camara, C., Oom, D., & Mota, B. (2008). Global fire activity patterns (1996–2006) and climatic influence: an analysis using the World Fire Atlas. *Atmospheric Chemistry and Physics*, 8(7), 1911–1924. https://doi.org/10.5194/acp-8-1911-2008

Leandro, J., & Martins, R. (2016). A methodology for linking 2D overland flow models with the sewer network model SWMM 5.1 based on dynamic link libraries. *Water Science and Technology*, 73(12), 3017–3026. https://doi.org/10.2166/wst.2016.171

Lee, R., White, C. J., Adnan, M. S. G., Douglas, J., Mahecha, M. D., O'Loughlin, F. E., Patelli, E., Ramos, A. M., Roberts, M. J., Martius, O., Tubaldi, E., van den Hurk, B., Ward, P. J., & Zscheischler, J. (2024). Reclassifying historical disasters: From single to multi-hazards. *Science of The Total Environment*, 912, 169120. https://doi.org/10.1016/j.scitotenv.2023.169120

Maggioni, M., & Gruber, U. (2003). The influence of topographic parameters on avalanche release dimension and frequency. *Cold Regions Science and Technology*, 37(3), 407–419. https://doi.org/10.1016/S0165-232X(03)00080-6

Maggioni, M., Gruber, U., & Stoffel, A. (2002). Definition and characterisation of potential avalanche release areas. ESRI Conference.

Maidment, D. R. (2017). Conceptual framework for the national flood interoperability experiment. *Journal of the American Water Resources Association*, 53(2), 245–257. https://doi.org/10.1111/1752-1688.12474

Margreth, S., Funk, M., Tobler, D., Dalban, P., Meier, L., & Lauper, J. (2017). Analysis of the hazard caused by ice avalanches from the hanging glacier on the Eiger west face. *Cold Regions Science and Technology*, 144, 63–72. https://doi.org/10.1016/j.coldregions.2017.05.012

Martha, T. R., Roy, P., Jain, N., Vinod Kumar, K., Reddy, P. S., Nalini, J., Sharma, S. V. S. P., Shukla, A. K., Durga Rao, K. H. V., Narender, B., Rao, P. V. N., & Muralikrishnan, S. (2021). Rock avalanche induced flash flood on 07 February 2021 in Uttarakhand, India—a photogeological reconstruction of the event. *Landslides*, 18(8), 2881–2893. https://doi.org/10.1007/s10346-021-01691-9

Marzocchi, W., Mastellone, M., Di Ruocco, A., Novelli, P., Romeo, E., & Gasparini, P. (2009). Principles of multirisk assessment: interactions amongst natural and man-induced risks.

Meral, A., & Yüksel, A. (2024). Çığ Kontrolü Projelendirme Çalışmalarında Risk Analizi Değerlendirmesi. E*ge 11th Uluslararası Uygulamalı Bilimler Kongresi*, 842–855.

Mesta, B., Sasaki, H., Nakaegawa, T., & Kentel, E. (2022). Changes in precipitation climatology for the Eastern Mediterranean using CORDEX RCMs, NHRCM and MRI-AGCM. *Atmospheric Research*, 272, 106140. https://doi.org/10.1016/j.atmosres.2022.106140

Met Office. (2014). Winter storms, January to February 2014.

MGM. (2025, January 14). Resmi iklim istatistikleri. https://mgm.gov.tr/veridegerlendirme/il-ve-ilceler-istatistik.aspx?k=undefined&m=bingol

Michoud, C., Derron, M. H., Horton, P., Jaboyedoff, M., Baillifard, F. J., Loye, A., Nicolet, P., Pedrazzini, A., & Queyrel, A. (2012). Rockfall hazard and risk assessments along roads at a regional scale: example in Swiss Alps. *Natural Hazards and Earth System Sciences*, 12(3), 615–629. https://doi.org/10.5194/nhess-12-615-2012

MTA. (2025). Yer bilimleri harita görüntüleyici ve çizim editörü. http://yerbilimleri.mta.gov.tr/anasayfa.aspx

Nadim, F., Liu, Z., Vagelsten, B. V., Aristizabal, A. G., Woo, G., Aspinall, W., Fleming, K., & van Gelder, P. (2014). MATRIX framework for multi-risk assessment. *In New Multi-Hazard and Multi-Risk Assessment Methods for Europe* (pp. 31–36). EU Report.

Namara, W. G., Damisse, T. A., & Tufa, F. G. (2022). Application of HEC-RAS and HEC-GeoRAS model for flood inundation Mapping, the case of Awash Bello Flood Plain, Upper Awash River Basin, Oromiya Regional State, Ethiopia. M*odeling Earth Systems and Environment*, 8(2), 1449–1460. https://doi.org/10.1007/s40808-021-01166-9

OGM. (2013). Murat Nehri Havzası Rehabilitasyon Projesi Lediz Mikrohavza Planı.

Pardini, G., Gispert, M., & Dunjo, G. (2003). Runoff erosion and nutrient depletion in five Mediterranean soils of NE Spain under different land use. *The Science of The Total Environment*, 309(1–3), 213–224. https://doi.org/10.1016/S0048-9697(03)00007-X

Pathan, A. I., & Agnihotri, P. G. (2021). Application of new HEC-RAS version 5 for 1D hydrodynamic flood modeling with special reference through geospatial techniques: a case of River Purna at Navsari, Gujarat, India. *Modeling Earth Systems and Environment*, 7(2), 1133–1144. https://doi.org/10.1007/s40808-020-00961-0

Pearson, C. M. (2016). Modelling the potential impact of spatially targeted natural flood management at the landscape scale for a rural UK catchment. Environmental Science, Geography, Engineering.

Peker, İ. B., Gülbaz, S., Demir, V., Orhan, O., & Beden, N. (2024). Integration of HEC-RAS and HEC-HMS with GIS in flood modeling and flood hazard mapping. *Sustainability*, 16, 1226.

Pourghasemi, H. R. (2016). GIS-based forest fire susceptibility mapping in Iran: a comparison between evidential belief function and binary logistic regression models. *Scandinavian Journal of Forest Research*, 31(1), 80–98. https://doi.org/10.1080/02827581.2015.1052750

Pourghasemi, H. R., Yousefi, S., Kornejady, A., & Cerdà, A. (2017). Performance assessment of individual and ensemble data-mining techniques for gully erosion modeling. *Science of The Total Environment*, 609, 764–775. https://doi.org/10.1016/j.scitotenv.2017.07.198

Pourtaghi, Z. S., Pourghasemi, H. R., Aretano, R., & Semeraro, T. (2016). Investigation of general indicators influencing on forest fire and its susceptibility modeling using different data mining techniques. *Ecological Indicators*, 64, 72–84. https://doi.org/10.1016/j.ecolind.2015.12.030

Prosdocimi, M., Cerdà, A., & Tarolli, P. (2016). Soil water erosion on Mediterranean vineyards: A review. *CATENA,* 141, 1–21. https://doi.org/10.1016/j.catena.2016.02.010

Rahmati, O., Yousefi, S., Kalantari, Z., Uuemaa, E., Teimurian, T., Keesstra, S., Pham, T., & Tien Bui, D. (2019). Multi-Hazard Exposure Mapping Using Machine Learning Techniques: A Case Study from Iran. *Remote Sensing*, 11(16), 1943. https://doi.org/10.3390/rs11161943

Rahmati, O., Zeinivand, H., & Besharat, M. (2016). Flood hazard zoning in Yasooj region, Iran, using GIS and multi-criteria decision analysis. Geomatics, *Natural Hazards and Risk*, 7(3), 1000–1017. https://doi.org/10.1080/19475705.2015.1045043

RAMMS. (2024). RAMMS::Avalanche user manual (v1.8.0). RAMMS.

Rijsdijk, A., Sampurno Bruijnzeel, L. A., & Sutoto, C. K. (2007). Runoff and sediment yield from rural roads, trails and settlements in the upper Konto catchment, East Java, Indonesia. *Geomorphology*, 87(1–2), 28–37. https://doi.org/10.1016/j.geomorph.2006.06.040

Rusk, J., Maharjan, A., Tiwari, P., Chen, T. K., Shneiderman, S., Turin, M., & Seto, K. C. (2022). Multi-hazard susceptibility and exposure assessment of the Hindu Kush Himalaya. *Science of The Total Environment*, 804, 150039. https://doi.org/10.1016/j.scitotenv.2021.150039

Sharma, A., & Miyazaki, H. (2019). Multi-hazard risk assessment in urban planning and development using AHP. The International Archives of the Photogrammetry, *Remote Sensing and Spatial Information Sciences*, 363–371.

Sharma, S., Talchabhadel, R., Nepal, S., Ghimire, G. R., Rakhal, B., Panthi, J., Adhikari, B. R., Pradhanang, S. M., Maskey, S., & Kumar, S. (2023). Increasing risk of cascading hazards in the central Himalayas. *Natural Hazards*, 119(2), 1117–1126. https://doi.org/10.1007/s11069-022-05462-0

Sovilla, B., McElwaine, J. N., & Köhler, A. (2018). The intermittency regions of powder snow avalanches. *Journal of Geophysical Research: Earth Surface*, 123(10), 2525–2545. https://doi.org/10.1029/2018JF004678

Spitz, W., Lagasse, P., Schumm, S., & Zevenbergen, L. (2001). A methodology for predicting channel migration NCHRP project no. 24-16. Wetlands Engineering & River Restoration 2001, 1–11. https://doi.org/10.1061/40581(2001)106

Suresh D., Yarrakula, K., Venkateswarlu B., Mohanty, B., & Manupati, V. (2019). Risk Mapping Analysis With Geographic Information Systems for Landslides Using Supply Chain. *In Emerging applications in supply chains for sustainable business development* (pp. 131–141). https://doi.org/10.4018/978-1-5225-5424-0.ch008

Tamiru, H., & Dinka, M. O. (2021). Application of ANN and HEC-RAS model for flood inundation mapping in lower Baro Akobo River Basin, Ethiopia. *Journal of Hydrology: Regional Studies*, 36, 100855. https://doi.org/10.1016/j.ejrh.2021.100855

Tarvainen, T., Jarva, J., & Greiving, S. (2006). Spatial pattern of hazards and hazard interactions in Europe. *In Natural and technological hazards and risks affecting the spatial development of European Regions* (pp. 83–91). Geological Survey of Finland.

Teng, J., Jakeman, A. J., Vaze, J., Croke, B. F. W., Dutta, D., & Kim, S. (2017). Flood inundation modelling: A review of methods, recent advances and uncertainty analysis. *Environmental Modelling & Software*, 90, 201–216.

Terzi, S., Torresan, S., Schneiderbauer, S., Critto, A., Zebisch, M., & Marcomini, A. (2019). Multi-risk assessment in mountain regions: A review of modelling approaches for climate change adaptation. *Journal of Environmental Management*, 232, 759–771. https://doi.org/10.1016/j.jenvman.2018.11.100

Tilloy, A., Malamud, B. D., Winter, H., & Joly-Laugel, A. (2019). A review of quantification methodologies for multi-hazard interrelationships. *Earth-Science Reviews*, 196, 102881. https://doi.org/10.1016/j.earscirev.2019.102881

Toro, E. F. (2001). Shock-capturing methods for free-surface shallow flows. Wiley.

Tsereteli, E., Gaprindashvili, G., Gaprindashvili, M., Bolashvili, N., & Gongadze, M. (2019). Hazard risk of debris/mud flow events in Georgia and methodological approaches for management. In IAEG/AEG Annual Meeting Proceedings, San Francisco, California, 2018 - Volume 5 (pp. 153–160). Springer International Publishing. https://doi.org/10.1007/978-3-319-93136-4_19

USACE. (2010). River analysis system HEC-RAS: Applications guide; hydrologic engineering center (HEC).

USACE. (2023). HEC-RAS 2D modeling user's manual. U.S. Army corps of engineers.

Van Westen, C. J., & Greiving, S. (2017). Multi-hazard risk assessment and decision making. In *Environmental Hazards Methodologies for Risk Assessment and Management* (pp. 31–94). IWA.

Wang, J., He, Z., & Weng, W. (2020). A review of the research into the relations between hazards in multi-hazard risk analysis. *Natural Hazards*, 104(3), 2003–2026. https://doi.org/10.1007/s11069-020-04259-3

WMO. (2009). Manual on estimation of probable maximum precipitation.

Yıldız, E., & Bulut, İ. (2024). Türkiye'de potansiyel çığ başlama bölgelerinin tespiti, çığ mobil uygulaması ve çığ tehlike haritalarının hazırlanması süreçleri: Palandöken Kayak Merkezi Örneği. *Çevre, Şehir ve İklim Dergisi*, Özel Sayı, 157–181.

Yousefi, S., Pourghasemi, H. R., Emami, S. N., Pouyan, S., Eskandari, S., & Tiefenbacher, J. P. (2020). A machine learning framework for multi-hazards modeling and mapping in a mountainous area. *Scientific Reports*, 10(1), 12144. https://doi.org/10.1038/s41598-020-69233-2

Youssef, A. M., Mahdi, A. M., & Pourghasemi, H. R. (2022). Landslides and flood multi-hazard assessment using machine learning techniques. *Bulletin of Engineering Geology and the Environment*, 81(9), 370. https://doi.org/10.1007/s10064-022-02874-x

Zhou, H., Wang, J., Wan, J., & Jia, H. (2010). Resilience to natural hazards: a geographic perspective. *Natural Hazards*, 53(1), 21–41. https://doi.org/10.1007/s11069-009-9407-y

Zscheischler, J., Westra, S., van den Hurk, B. J. J. M., Seneviratne, S. I., Ward, P. J., Pitman, A., AghaKouchak, A., Bresch, D. N., Leonard, M., Wahl, T., & Zhang, X. (2018). Future climate risk from compound events. *Nature Climate Change*, 8(6), 469–477. https://doi.org/10.1038/s41558-018-0156-3